Evaluation of the seasonal formation of subsurface negative preformed nitrate anomalies in the subtropical North Pacific and North Atlantic

Robert T. Letscher[1*] and Tracy A. Villareal[2]

[1]Earth Sciences and Ocean Process Analysis Laboratory, University of New Hampshire, Durham, NH, USA 03824

[2]Department of Marine Science and Marine Science Institute, The University of Texas, Austin, Port Aransas, Austin, TX, USA 78382

*Correspondance email: robert.letscher@unh.edu

Abstract

Summertime mixed-layer drawdown of dissolved inorganic carbon in the absence of measurable nutrients in the ocean's subtropical gyres and non-Redfieldian oxygen:nitrate relationships in the underlying subsurface waters are two biogeochemical phenomena that have thus far eluded complete description. Many processes are thought to contribute to one or both including lateral nutrient transport, carbon overconsumption or non-Redfield C:N:P organic matter cycling, heterotrophic nutrient uptake, and the actions of vertically migrating phytoplankton. To obtain insight into the likely magnitude of potential contributing mechanisms, we investigated the seasonal formation rates for negative preformed nitrate ($preNO_3$) anomalies (oxygen consumption without stoichiometric nitrate release) in the subsurface and positive preformed nitrate anomalies (oxygen production without stoichiometric nitrate drawdown) in the euphotic zone at the subtropical ocean time series stations ALOHA in the North Pacific and BATS in the North Atlantic. Non-Redfield $-O_2$:N stoichiometry for dissolved organic matter (DOM) remineralization is found to account for up to ~15 mmol N m^{-2} yr^{-1} of negative $preNO_3$ anomaly formation at both stations. Residual negative anomalies in excess of that which can be accounted for by non-Redfield DOM cycling are found to accumulate at a rate of ~32 – 46 mmol N m^{-2} yr^{-1} at station ALOHA and ~46 – 87 mmol N m^{-2} yr^{-1} at the BATS station. These negative anomaly formation rates are in approximate balance with residual positive $preNO_3$ anomaly formation rates from the euphotic zone located immediately above the nutricline in the water column. Using the limited literature available, we calculate that cycling of transparent exopolymer particles (TEP) and heterotrophic nitrate uptake can contribute to the formation of these residual $preNO_3$ anomalies; however, a significant fraction, estimated at ~50 – 95%, is unexplained by the sum of these processes. Vertically migrating phytoplankton possess the

necessary distribution, nutrient acquisition strategy and biogeochemical signature to potentially explain both the negative and positive residual preNO_3 anomalies as well as the mixed layer dissolved inorganic carbon drawdown at stations ALOHA and BATS. However, the processes examined are not independent and mutually exclusive. The model *Rhizosolenia* mat system (and perhaps other migrators) produce TEP and migration could provide accelerated vertical transport of TEP as well as provide labile carbon for heterotrophic nitrate uptake. These results based on geochemical distributions suggest that in the absence of additional mechanisms and rates, phytoplankton vertical migrators, although rare and easily overlooked, play a larger role in subtropical ocean nutrient cycling and the biological pump than generally recognized.

Introduction

Subtropical ocean gyre ecosystems exhibit low rates of primary productivity caused by thermal stratification of the water column that acts as an impediment to sustained nutrient supply to the surface ocean. Yet these regions exhibit significant annual net community production (ANCP), estimated at 3 ± 1 mol C m^{-2} yr^{-1} for station ALOHA in the North Pacific (Hawaii Ocean Time-series) and the BATS station (Bermuda Atlantic Time-Series) in the North Atlantic (Emerson, 2014), contributing about half of the global biological carbon pump (Emerson et al., 1997). Observations at these two well-characterized time-series sites indicate a seasonal drawdown of mixed layer dissolved inorganic carbon (DIC) occurs during the summer and early autumn months that is attributed to net community production with minor contributions from lateral mixing and air-sea CO_2 exchange (Gruber et al., 1998, 2002; Keeling et al., 2004; Williams et al., 2013).

69 The nutrient sources supporting this seasonal DIC drawdown at the time-series sites have
70 eluded oceanographers since the phenomenon was first documented (Michaels et al., 1994;
71 Toggweiler, 1994; Gruber et al., 1998; Keeling et al., 2004). Numerous nutrient input
72 mechanisms have been investigated including vertical mixing, N_2 fixation, atmospheric
73 deposition, and eddy movements with their sum still falling short of explaining the observed DIC
74 drawdown or a stoichiometric equivalent subsurface oxygen consumption (Jenkins and
75 Goldman, 1985; Jenkins and Doney, 2003) assuming Redfield stoichiometry between organic
76 matter production and remineralization. More recently, episodic vertical mixing events and
77 lateral advection are two physical mechanisms that have been proposed to supply the surface
78 subtropical gyres with the "missing" nutrients to explain observed ANCP (Johnson et al., 2010;
79 Letscher et al., 2016). However, in order to explain the observed summertime DIC drawdown
80 from the subtropical gyre mixed layer, these two physical mechanisms must supply nutrients,
81 carbon, and oxygen in non-Redfield stoichiometries. Letscher et al. (2016) reported C-deficient,
82 non-Redfieldian supply of inorganic carbon and nutrients within the lateral nutrient streams
83 reaching the subtropical gyres; however, this mechanism still falls short of explaining the
84 observed DIC drawdown at stations ALOHA and BATS, even after accounting for non-Redfield
85 C:N:P stoichiometry of organic matter production. Johnson et al. (2010) used profiling floats
86 equipped with biogeochemical sensors to observe episodic, near monthly, vertical mixing events
87 near station ALOHA that supply nitrate from the nitracline upwards into the euphotic zone to a
88 depth of ~75-100 m. To explain the surface DIC drawdown, these authors suggested the non-
89 Redfieldian supply of nitrate into the mixed layer above ~50 m could be carried out by large,
90 non-flagellated phytoplankton that migrate between the nutricline and the surface as part of their
91 life-history strategy for nutrient acquisition (Villareal et al., 1993; 2014). Multiple lines of

evidence indicate that this subset of the oceanic flora is migrating (Villareal et al., 2014) and transports new nitrogen into the euphotic zone (Villareal et al., 1993; Richardson et al., 1998; Villareal et al., 1996). As an analogy, migration by flagellated phytoplankton in coastal waters is sufficient to alter geochemical properties. Fraga et al. (1992, 1999) observed that the flagellated coastal dinoflagellate *Gymnodinium catenatum* transports nutrients via vertical migration in relaxed upwelling conditions and developed modifications to Broeker's (1974) NO tracer that expressed how the dinoflagellate migration modifies geochemical properties. In the open ocean, giant phytoplankton (up to 10^9 μm^3) can overcome the much greater distances (~50–100 m) required to access the spatially segregated resource fields (light and nutrients) with size related ascent and descent rates. The challenge has been to quantify the various taxa's role in nitrate transport since this group is difficult to enumerate and abundance data is quite limited (Villareal et al., 2014).

In conjunction with the "missing" nutrient supply required to explain observed mixed layer DIC drawdown, the subtropical gyre regions also exhibit a deficit of sub-euphotic zone nitrate as expected from observed oxygen consumption and Redfield $-O_2$:N organic matter remineralization stoichiometry. This phenomenon is revealed when examining spatiotemporal patterns of the preformed nitrate ($preNO_3$) tracer. $preNO_3$ is traditionally calculated as $preNO_3 = NO_{3meas} - AOU/R_{-O2:N}$, where AOU is the apparent oxygen utilization and $R_{-O2:N}$ is the stoichiometric ratio of oxygen consumed to N regenerated for the remineralization of Redfieldian organic matter, e.g. 150:16 (9.4; Anderson, 1995). $preNO_3$ quantifies the fraction of measured nitrate in a water parcel not attributable to remineralization of Redfieldian organic matter and was initially formulated as a conservative tracer for examining the distribution of water masses involved in the global thermohaline circulation (Broecker, 1974). However, observations of

115 preNO$_3$ within upper mesopelagic depths (~100-300 m) of the subtropical ocean have revealed
116 negative preNO$_3$ (NPN) anomalies, suggesting there are non-Redfieldian processes affecting the
117 *in situ* dissolved oxygen and nitrate pools as well (Abell et al., 2005; Johnson et al., 2010). That
118 is, the observed negative anomalies are the result of oxygen consumption without concurrent
119 Redfieldian nitrate accumulation. Abell et al. (2005) suggested production, export, and
120 remineralization of dissolved organic matter (DOM) with non-Redfield, elevated C:N
121 stoichiometry could quantitatively explain the subsurface preNO$_3$ distribution in the subtropical
122 North Pacific. Working in the same ecosystem, Johnson et al. (2010) suggested that the
123 subsurface NPN anomaly (calculated using a modified Redfield ratio) could be sustained by
124 vertical separation between nitrate uptake in the nutricline and oxygen production/net
125 community production near the surface. Their data supported the conclusion that the upper 250
126 m is in approximate balance between nutrient supply and demand, suggesting that there are
127 processes that redistribute nitrate within this region. In the absence of other mechanisms, they
128 suggested that the observed mixed layer net community production is mediated by 1) directly
129 observed episodic vertical physical mixing events that deliver nitrate above 125 m and 2)
130 inferred transport by vertically migrating phytoplankton transporting this nitrate upwards along a
131 near-zero concentration gradient within the euphotic zone. Additional hypotheses advanced to
132 explain the DIC drawdown and/or the subsurface NPN anomaly include heterotrophic uptake of
133 nitrate and spatially segregated transparent exopolymer (TEP) production and consumption. To
134 date, no work has attempted to partition the contribution of the various mechanisms to formation
135 of the negative preNO$_3$ anomaly in subtropical ocean gyre systems..

136 In this work, we expand the examination of preNO$_3$ anomalies to the BATS station in the
137 North Atlantic and revisit the missing nutrient and NPN anomaly problems at both stations

ALOHA and BATS. We update the calculation of $preNO_3$ to explicitly include the contribution of DOM and its non-Redfield $-O_2$:N remineralization stoichiometry to the subsurface tracer fields in a manner analogous to Abell et al. (2005). Using this revised $preNO_3$ calculation, we define the residual $preNO_3$ tracer, which quantifies the $preNO_3$ distribution not attributable to the non-Redfield $-O_2$:N DOM remineralization stoichiometry mechanism. Seasonal formation of a sub-euphotic zone residual negative $preNO_3$ (rNPN) anomaly at the BATS station and a persistent sub-euphotic zone rNPN anomaly at station ALOHA are identified within the nutricline, similar to previous work in the subtropical North Pacific (Abell et al., 2005; Johnson et al., 2010). In addition, residual positive $preNO_3$ (rPPN) anomalies are observed within the euphotic zone (0 – ~80 or ~100 m) at both sites, with integrated rates of formation that are in approximate stoichiometric balance with the rNPN anomalies located immediately below in the water column. These rNPN and rPPN anomalies account for the effects of both particulate organic matter (POM) and DOM remineralization with elevated $-O_2$:N stoichiometry, thus requiring additional mechanisms for their formation. We undertake a quantitative examination of other potential contributing mechanisms to explain the subsurface rNPN anomalies, euphotic zone rPPN anomalies, and mixed layer DIC drawdown including transparent exopolymer particle (TEP) cycling, subsurface bacterial uptake of nitrate, and vertical migration by phytoplankton. We find that TEP cycling may explain a fraction of both the rNPN and rPPN anomalies; bacterial nitrate uptake accounts for only a small fraction of rNPN and none of the rPPN anomalies. In the absence of additional unknown mechanisms, phytoplankton vertical migration contributes the dominant flux of N to explain both the rNPN (via nitrate consumption and upward transport) and rPPN (via oxygen production during internal nitrate consumption) anomalies at both stations ALOHA and BATS. The observed rates at the time-series sites are within the range of previously

estimated vertical transport rates elsewhere in the subtropical ocean. In addition, the observed production of TEP by migrating diatom mats (and by inference, other migrators) provides a linkage between at least two of the processes. These calculations provide a framework for evaluating the role of these processes in future studies.

Methods

Data

Time-series biogeochemical data including concentrations of total dissolved nitrogen, nitrate + nitrite, and oxygen for the years 1988-2016 were downloaded from http://bats.bios.edu for the BATS station and http://hahana.soest.hawaii.edu/hot for Station ALOHA. Dissolved organic nitrogen (DON) was calculated as total dissolved nitrogen (GF/F 0.7 μm filtered) minus [nitrate + nitrite]. This definition of DON includes ammonium; however, its open ocean concentration is typically < 50 nM and is not regularly measured as part of the two time-series. Global annual climatologies for dissolved O_2 and NO_3^- from the World Ocean Atlas (WOA) 2013 (Garcia et al., 2014a; 2014b) were downloaded from http://www.nodc.noaa.gov/OC5. The Global Ocean Data Analysis Project (GLODAP) v2 dataset (Olsen et al. 2016) including dissolved O_2, NO_3^-, CFC-11, and CFC-12 was downloaded from http://www.nodc.noaa.gov/ocads/oceans/GLODAPv2. The WOA and GLODAP data products provide our analysis with an annual time-mean picture of thermocline preNO_3 tracer distributions across the larger spatial scales of the North Atlantic, North Pacific, and the other subtropical gyre regions of the global ocean. Water mass ventilation ages on subsurface neutral density layers are computed from the GLODAP v2 CFC-11 and CFC-12 data using a method similar to that described in Doney and Bullister (1992) using the atmospheric time-history of the CFC gases

184 provided by Walker et al. (2000) and the gas solubility constants of Warner and Weiss (1985).
185 All calculations of rNPN and rPPN anomaly formation rates at the time-series sites are
186 performed from analysis of the monthly-resolved Station ALOHA and BATS datasets.
187
188 **Tracer computations**
189 The preformed NO_3 tracer defined by Broecker (1974) separates the observationally
190 determined nitrate concentration for a given water parcel into contributions from water mass
191 mixing (preformed) and regenerated from respiration of organic matter. Traditional formulations
192 of preNO_3 assign a uniform $-O_2$:NO_3 stoichiometry, e.g. 9.0 (Broecker, 1974), of organic matter
193 remineralization without discriminating between particulate vs. dissolved organic matter (DOM)
194 pools. However, Abell et al. (2005) showed that DOM remineralization stoichiometry is
195 significantly elevated with respect to Redfield proportions in the subtropical North Pacific, with
196 $-O_2$:N stoichiometries of 23 to 30 within shallow mesopelagic density layers (σ_θ = 24.4 – 26.1)
197 compared to Redfield values of 6.9 to 10.6 (Takahashi et al., 1985; Martin et al., 1987; Anderson
198 and Sarmiento, 1994; Paulmier et al., 2009). This required an additional term in the calculation
199 of preNO_3 in their analysis, accounting for the fraction of oxygen consumption attributable to
200 DOM remineralization and its separate stoichiometry. Abell et al. (2005) inferred the subsurface
201 $-O_2$:N stoichiometry of DOM remineralization from regressions of observed O_2 vs. dissolved
202 organic carbon (DOC) concentrations within upper mesopelagic isopycnal layers. The regression
203 was converted to N units with the separately measured DOC:DON ratio. Here we adopt the Abell
204 et al. (2005) analysis and directly estimate the $-O_2$:N stoichiometry of dissolved organic nitrogen
205 remineralization within upper mesopelagic density layers at stations ALOHA and BATS to
206 compute the residual preNO_3 tracer.

The residual $preNO_3$ tracer formulation including the effects of DOM remineralization is:

$$residual\ preNO_3 = NO_{3meas} - \left(f_{DOM} \cdot \frac{AOU}{rDOM}\right) - \left(f_{POM} \cdot \frac{AOU}{rPOM}\right) \quad (1)$$

NO_{3meas} is the sum of dissolved nitrate + nitrite. Apparent oxygen utilization (AOU) is calculated as $AOU = O_{2sat} - O_{2meas}$; the difference between O_2 saturation at a given temperature, salinity, and pressure with the observationally determined O_2 concentration. The two DOM terms, f_{DOM}, the fraction of oxygen consumption attributable to DOM remineralization and r_{DOM}, the stoichiometric ratio of O_2 consumed per mole of DON remineralized, can be determined empirically from the time-series O_2 and DON data. Values of r_{DOM} were determined empirically each year between 1989 – 2000 at Station ALOHA and 1993 – 2016 at the BATS station by Model II linear regression (Ricker, 1973; Trujillo-Ortiz and Hernandez-Walls, 2010) of AOU vs. DON within discrete neutral density layers. The subsurface neutral density layers $\gamma^n = 24.2 – 24.7$ and $\gamma^n = 24.7 – 25.2$ were chosen at station ALOHA and $\gamma^n = 25.8 – 26.3$ at the BATS station for subsequent calculation of DOM $–O_2$:N remineralization stoichiometry based on a first examination of the depths exhibiting NPN anomalies using the traditional (Redfieldian) formulation of the $preNO_3$ tracer, i.e. $preNO_3 = NO_{3meas} – AOU/R_{-O2:N}$. with the value of $R_{-O2:N}$ selected as 150:16 (Anderson, 1995). The fraction of oxygen consumption attributable to DOM remineralization, f_{DOM}, is determined empirically for each neutral density layer following the equation of Abell et al. (2000):

$$f_{DOM} = \frac{\Delta DOM}{\Delta DOM + \Delta POM} = \frac{rPOM}{rDOM} \quad (2)$$

The stoichiometric ratio of O_2 consumed per mole of particulate organic nitrogen (PON) remineralized, r_{POM}, cannot be uniquely determined from Eq. 2 or the time-series data and is taken from the literature (6.9 to 10.6; Paulmier et al., 2009). We used the climatological average r_{DOM} in Eq. 2 due to a reduced number of years exhibiting statistically significant regressions of

AOU vs. DON. Years with a regression correlation coefficient > 0.33 were included in the climatological average (~55% of years investigated). Thus, our approach assumes r_{DOM} and f_{DOM} are constant over time within each density horizon investigated at each station. Relative uncertainty in the literature values of r_{POM} is larger (~55%) than the computed uncertainty in r_{DOM} (~33%). The last remaining term in Eq. 1, f_{POM}, the fraction of AOU attributable to POM remineralization, is calculated as $1 - f_{DOM}$. We tested the sensitivity of our computed residual $preNO_3$ from Eq. 1 and 2 by allowing r_{POM} to vary from 6.9 to 10.6, the upper and lower bound values for r_{POM} reported in the literature (Paulmier et al., 2009).

The seasonal formation rate of rNPN anomalies at each time-series site were estimated by a linear regression of the residual $preNO_3$ tracer vs. time within the aforementioned subsurface neutral density layers for the years 1989-2016 at Station ALOHA and 1993-2016 at the BATS station. The slope of this regression yields the volumetric rate of rNPN anomaly formation in units of μmol N m^{-3} d^{-1}. The volumetric rates were depth and time integrated to provide annual rates of rNPN anomaly formation in units of mmol N m^{-2} yr^{-1}. Depth integration was performed by estimating the thickness, H, each year of the subsurface neutral density layers at the BATS and ALOHA stations. Values of H varied between 20 to 100 m. Time integration was calculated from the number of days elapsed between the first observation of decreasing residual $preNO_3$ values to the date when residual $preNO_3$ ceased decreasing within the annual cycle (Fig. S1, S2, S4). The volumetric rates of rPPN formation within the euphotic zone and their depth integration at each time-series site were performed within the 0 – 100 m layer at Station ALOHA and within the 0 – 80 m layer at the BATS station. Time integration for rPPN anomalies was performed analogously to rNPN anomalies; from the time elapsed between observations of increasing residual $preNO_3$ within the euphotic zone over the annual cycle (Fig. S3, S5). For the calculation

of the residual preNO$_3$ tracer within the euphotic zone, we made the assumption that the values of f_{DOM} and r_{DOM} were equivalent to those empirically derived for the upper mesopelagic density layer present immediately below the euphotic zone at each site. Seasonal rNPN anomaly formation duration ranged from a minimum of 2 months to a maximum of 10.5 months with a median of 7.5 months. Seasonal rPPN anomaly formation duration ranged from a minimum of 4 months to a maximum of 10 months with a median of 6 months.

A residual preformed phosphate (prePO$_4$) tracer was computed as:

$$residual\ prePO_4 = PO_{4meas} - \left(f_{DOM} \cdot \frac{AOU}{rDOM}\right) - \left(f_{POM} \cdot \frac{AOU}{rPOM}\right)$$

Dissolved organic phosphorus concentration data density was not sufficient to allow for statistically significant regressions of AOU versus DOP needed to empirically estimate f_{DOM} and r_{DOM} terms specific to DOP remineralization at each site. To compute prePO$_4$ for each station, we used the values of f_{DOM}, r_{DOM}, and r_{POM} from Table 1 calculated from regressions of AOU vs. DON, converting from N units to P units using a DON:DOP ratio of 16:1 for semilabile DOM remineralization in the subtropical North Atlantic and North Pacific (Letscher & Moore, 2015).

Results

DOM remineralization in the upper mesopelagic at the ALOHA and BATS stations

Empirically derived, annual values of r_{DOM} at Station ALOHA varied between 10.4 and 24.2 for the γ^n = 24.2 – 24.7 layer and between 12.7 and 23.5 for the γ^n = 24.7 – 25.2 layer. Values of r_{DOM} at the BATS station varied between 14.0 and 25.3 in the γ^n = 25.8 – 26.3 layer. Climatological average r_{DOM} computed for each density layer yielded ratios of 18.1 to 18.9 at Station ALOHA and 21.1 at the BATS station (Table 1; standard errors on r_{DOM} are on the order of 33%). These climatological values of r_{DOM} were used in subsequent calculations of residual

preNO$_3$ and f_{DOM} from equations 1 and 2. The empirically derived values of r_{DOM} are consistently larger than the literature estimates of r_{POM}, indicating that remineralization of DOM in the upper mesopelagic returns less moles of nitrate per mole of O_2 respired at the two sites compared to Redfield stoichiometry.

Empirically derived values of f_{DOM} varied between 0.38 and 0.59 for the γ^n = 24.2 – 24.7 layer and between 0.36 and 0.6 for the γ^n = 24.7 – 25.2 layer at station ALOHA. Values of f_{DOM} at the BATS station varied between 0.33 and 0.5 in the γ^n = 25.8 – 26.3 layer. Climatological average f_{DOM} values of 0.5 for both density layers at station ALOHA and a value of 0.4 at the BATS station (Table 1) were used in subsequent calculation of residual preNO$_3$ from Equation 1.

Upper ocean residual preNO$_3$ climatology at the ALOHA and BATS stations

Station ALOHA – The climatology of the residual preNO$_3$ [µM] tracer (the amount remaining after accounting for DOM contributions to AOU) is presented for the upper 250 m at Station ALOHA in Figure 1a. Residual preNO$_3$ varies between -1 to 1 µM in the upper ~200 m with increasingly positive values below 200 m. The resulting rNPN anomaly (blue colors) is a persistent feature within the 24.2 – 25.2 neutral density layer at a depth of ~100 to 200 m. Seasonal rPPN anomalies (red colors) are observed immediately above the 24.2 neutral density horizon within the euphotic zone, 0 to ~100 m. Pulses of rPPN anomalies penetrating the bottom of the rNPN anomaly layer are also observed that coincide with shoaling of the 25.2 neutral density horizon above 200 m.

The monthly averaged climatology of residual preNO$_3$ [µM] at Station ALOHA for all data in years 1989 – 2016 is presented in Figure 1b. The subsurface rNPN anomaly is observed to grow in magnitude between the months of May/June through Oct/Nov. There also exists an

increase in the magnitude of the rPPN anomaly within the euphotic zone (0 – 100 m), concomitant with the rNPN anomaly formation at ~100 – 200 m depth in summer.

Volumetric rates of rNPN anomaly formation at Station ALOHA are estimated at 2.8 ± 1.4 and 3.0 ± 1.5 μmol N m^{-3} d^{-1} for the γ^n = 24.2 – 24.7 layer using r_{POM} values of 6.9 and 10.6, respectively (Table 1). Slightly lower rates of rNPN anomaly formation of 1.6 ± 0.8 and 2.5 ± 1.4 μmol N m^{-3} d^{-1} are estimated for the deeper γ^n = 24.7 – 25.2 layer at Station ALOHA (annual regressions are provided in Fig. S1 & S2). Depth and time integrated, the estimates of rNPN anomaly formation become 28.3 ± 9.6 (r_{POM} = 6.9) and 17.9 ± 7.4 (r_{POM} = 10.6) mmol N m^{-2} yr^{-1} for the γ^n = 24.2 – 24.7 layer and 18.1 ± 8.8 (r_{POM} = 6.9) and 13.7 ± 7.8 (r_{POM} = 10.6) mmol N m^{-2} yr^{-1} for the deeper γ^n = 24.7 – 25.2 layer. Total rNPN formation rate estimates for Station ALOHA are between 31.6 ± 10.8 to 46.4 ± 13.0 mmol N m^{-2} yr^{-1} (Table 1).

The volumetric rate of rPPN anomaly formation within the euphotic zone at Station ALOHA is estimated at 3.3 ± 1.1 and 2.4 ± 0.8 μmol N m^{-3} d^{-1} using r_{POM} values of 6.9 and 10.6, respectively (Table 1, Fig. S3). These rates are approximately equivalent within error of those estimated for rNPN formation rate within the γ^n = 24.2 – 24.7 layer immediately below in the water column. Depth and time integrated, the estimate of rPPN anomaly formation is 61.2 ± 20.2 (r_{POM} = 6.9) and 43.5 ± 10.5 (r_{POM} = 10.6) mmol N m^{-2} yr^{-1} (Table 1). The euphotic zone integrated rPPN anomaly is approximately 33% higher than the estimated total integrated rNPN anomaly within the combined γ^n = 24.2 – 25.2 layer.

BATS – The climatology of the residual $preNO_3$ [μM] tracer in the upper 200 m at BATS is presented in Figure 2a. Residual $preNO_3$ varies between -1 to 1 μM in the upper 200 m and seasonal subsurface rNPN anomalies at ~80 to 160 m depth are observed in most but not all years from 1993 to 2016. Similar to Station ALOHA, seasonal pulses of rPPN anomalies are

observed immediately above the 25.8 neutral density horizon within the euphotic zone, 0 to ~80 m. Pulses of rPPN anomalies penetrating from below the 26.3 neutral density horizon are present in a few years but are much less frequent than observed in the Station ALOHA climatology. rPPN anomalies are observed immediately below the rNPN layer beginning at ~160 m.

The monthly averaged climatology of residual preNO_3 [μM] at BATS for all data in years 1993 – 2016 is presented in Figure 2b. The subsurface rNPN anomaly is observed to first appear beginning in Apr/May and grow in magnitude through the end of the calendar year. The rNPN feature starts shallow at a depth of ~60 to 100 m that deepens over the summer months to depths of ~80 to 160 m by years' end. There also exists a layer of rPPN anomaly at 0 – ~80 m depth that increases in magnitude, concomitant with the rNPN anomaly formation at ~80 – 160 m depth in summer and autumn. Late winter convective overturn of the upper water column in late Jan/Feb at the BATS station (Hansell and Carlson, 2001) erases both the subsurface rNPN and 0-80 m rPPN anomaly.

The volumetric rate of rNPN anomaly formation at the BATS station is estimated at 5.5 ± 2.7 and 3.8 ± 3.1 μmol N m^{-3} d^{-1} for the γ^n = 25.8 – 26.3 layer using r_{POM} values of 6.9 and 10.6, respectively (Table 1, Fig. S4). Depth and time integrated, the estimate of rNPN anomaly formation rate at the BATS station is between 46.0 ± 39.3 to 87.1 ± 41.0 mmol N m^{-2} yr^{-1} (Table 1). The volumetric rate of rPPN anomaly formation within the euphotic zone at the BATS station is estimated at 5.8 ± 1.2 and 4.1 ± 0.8 μmol N m^{-3} d^{-1} using r_{POM} values of 6.9 and 10.6, respectively (Table 1, Fig. S5). These rates are approximately equivalent within error of those estimated for rNPN formation rate within the γ^n = 25.8 – 26.3 layer immediately below in the water column. Depth and time integrated, the estimate of rPPN anomaly formation is 82.1 ± 13.8 (r_{POM} = 6.9) and 61.8 ± 12.2 (r_{POM} = 10.6) mmol N m^{-2} yr^{-1} (Table 1). The euphotic zone

integrated rPPN anomaly is approximately balanced (r_{POM} = 6.9) or 33% higher (r_{POM} = 10.6) than the estimated integrated rNPN anomaly within the γ^n = 25.8 – 26.3 layer.

Upper ocean residual $prePO_4$ climatology at the ALOHA and BATS stations

Station ALOHA – The climatology of the residual $prePO_4$ [μM] tracer is presented for the upper 250 m at Station ALOHA in Figure 3a. Residual $prePO_4$ varies between -0.04 to 0.2 μM with positive values observed throughout the upper 250 m of the time-series with exception of a period exhibiting small (~0 – -0.04 μM) residual negative $prePO_4$ anomalies at ~125 – 175 m in years 2002 – 2004. The monthly averaged climatology of residual $prePO_4$ [μM] at Station ALOHA for all data in years 1989 – 2016 is presented in Figure 3b. Positive residual $prePO_4$ (0 – 0.2 μM) is observed throughout the upper 250 m within the monthly averaged climatology.

BATS – The climatology of the residual $prePO_4$ [μM] tracer in the upper 200 m at BATS is presented in Figure 4a. Residual $prePO_4$ varies between -0.2 to 0.2 μM in the upper 200 m. Seasonal subsurface residual negative $prePO_4$ anomalies at ~80 to 160 m depth are observed in all years from 1993 to 2016 with the exception of 2015. Seasonal pulses of residual positive $prePO_4$ anomalies (~0 – 0.1 μM) are observed immediately above the 25.8 neutral density horizon within the euphotic zone, 0 to ~80 m.

The monthly averaged climatology of residual $prePO_4$ [μM] at BATS for all data in years 1993 – 2016 is presented in Figure 4b. The subsurface residual $prePO_4$ anomaly is present throughout the seasonal cycle although it is observed to grow in magnitude beginning in May continuing through the end of the calendar year into Jan/Feb, before springtime vertical overturning circulation resets the residual $prePO_4$ concentration in the upper 200 m. The residual negative $prePO_4$ feature starts shallow at a depth of ~80 m in May/Jun that deepens over the

summer months to depths of ~80 to 200 m by years' end. There also exists a layer of residual positive $prePO_4$ anomaly at 0 – ~80 m depth that develops during Apr – Nov, concomitant with the seasonally increasing residual negative $prePO_4$ anomaly at ~80 – 200 m depth in summer and autumn.

Discussion

Our analysis found DOM remineralization within the upper mesopelagic to follow non-Redfield $-O_2$:N stoichiometry at Station ALOHA (~18–19) and the BATS station (~21). However, contrary to the findings of Abell et al., (2005) working in the subtropical North Pacific, this mechanism cannot quantitatively explain the negative $preNO_3$ anomaly present in the subsurface. Instead, we find the euphotic zone to exhibit residual positive $preNO_3$ anomalies and the upper mesopelagic exhibits residual negative $preNO_3$ anomalies at Stations ALOHA and BATS. Our directly diagnosed DOM $-O_2$:N remineralization stoichiometry from observations of AOU and DON is significantly lower than that inferred by Abell et al. (2005) (~23–30) diagnosed from AOU vs. DOC remineralization stoichiometry and likely explains this discrepancy. Thus, the fraction of AOU attributable to DOM remineralization and its AOU vs. DON stoichiometry needs to be accounted for in any study that utilizes the $preNO_3$ tracer. The traditional $preNO_3$ tracer calculation should be abandoned and replaced with the residual $preNO_3$ tracer formulation as defined in our study (Eq. 1).

We now undertake a quantitative examination of the potential contributing mechanisms to explain the subsurface rNPN anomalies and euphotic zone rPPN anomalies.

Physical mechanisms

Both the ALOHA and BATS station climatologies of the residual preNO_3 tracer exhibit annual cycles of rPPN anomaly formation in the euphotic zone and subsurface rNPN anomaly formation beginning at ~100 m (ALOHA) or ~80 m (BATS) that intensifies from early summer through to mid-autumn (Fig. 1 and 2). This timeframe coincides with the period of thermal stratification of the water column at the BATS station, separating the surface mixed layer, ~0 – 30 m, from the deep chlorophyll max (DCM) present at ~100 – 120 m (Navarro and Ruiz, 2013). Station ALOHA exhibits year-round stratification with the deep chlorophyll max present at ~125 m (Navarro and Ruiz, 2013). The largest rPPN anomalies are observed in the vertical zone between the surface mixed layer and the DCM at both sites, at a depth of ~50 – 100 m at station ALOHA and a depth of ~40 – 80 m at the BATS station. This vertical zone of rPPN anomaly formation coincides with the observed subsurface O_2 maximum (SOM) that has historically been a conundrum to biogeochemical explanation given the *in situ* ^{14}C-diagnosed net primary production estimates (e.g. Jenkins and Goldman, 1985; Shulenberger and Reid, 1981; Platt et al., 1989). Our rPPN volumetric rates of formation converted to O_2 units using the values in Table 1 are approximately 20 – 37% (at Station ALOHA) of the estimated SOM formation rate in the subtropical central North Pacific and ~34 – 41% (at the BATS station) of the estimated SOM formation rate in the Sargasso Sea (Shulenberger and Reid, 1981).

Subsurface rNPN anomalies begin to appear at a depth of ~100 m at station ALOHA and ~80 m at the BATS station continuing down to depths of ~200 m and ~160 m, respectively. We estimated the depth of the top of the nitracline by defining this as the depth where $[NO_3^- + NO_2^-]$ = 0.5 μM in the monthly averaged climatologies. At Station ALOHA, the top of the nitracline varies between 120 – 130 m depth with a mean of ~126 m over the annual cycle. At the BATS station, the top of the nitracline varies between 90 – 120 m depth with an annual mean of ~102

413 m. Thus, the formation of rNPN anomalies is concurrent with the depth in the water column
414 where nitrate begins to accumulate from remineralization processes at both sites and continues to
415 form deeper into the nitracline.

416 What is the role of lateral physical mixing in creating the observed rPPN and rNPN
417 anomalies? To address this question, we turn to the World Ocean Atlas annual O_2 and NO_3^-
418 climatologies (Garcia et al., 2014a; 2014b) on the subsurface isopycnals present in the ~100 –
419 250 m depth layer at each site. We computed the residual $preNO_3$ tracer for the subtropical North
420 Pacific using the values of f_{DOM} and r_{DOM} for Station ALOHA and for the subtropical North
421 Atlantic using the values for the BATS station in Table 1. Examination of the residual $preNO_3$
422 tracer on the $\gamma^n = 26.5$ density surface (the surface approximately bisecting the 150 – 200 m layer
423 near BATS exhibiting rPPN anomalies) reveals that the BATS station is immediately surrounded
424 by waters with a residual $preNO_3$ value of ~1 μM (blue colors; Fig. S6). Waters with a residual
425 $preNO_3$ content of ~2 – 3 μM are present to the southwest and to the northeast (red colors, Fig.
426 S6). The lack of a residual $preNO_3$ gradient on the $\gamma^n = 26.5$ density surface in the immediate
427 vicinity of the BATS station suggests the observed ~1 μM residual $preNO_3$ concentration present
428 at ~150 – 200 m depth in Figure 2 represents a local signal with little mixing of waters with
429 different residual $preNO_3$ content. Lateral advective mixing of the higher residual $preNO_3$ waters
430 to the southwest and northeast of the BATS station would increase the residual $preNO_3$ on $\gamma^n =$
431 26.5 to values greater than 1 μM at the BATS station, which is not observed. Plots of residual
432 $preNO_3$ versus the CFC-11 and CFC-12 age on $\gamma^n = 26.5$ in the North Atlantic reveal essentially
433 no increasing or decreasing residual $preNO_3$ age gradient (Fig. S6). In summation, this evidence
434 suggests the BATS station sits within the NW corner of a large region of the subtropical North

435 Atlantic characterized by a residual preNO$_3$ content of ~1 μM on γ^n = 26.5 that is generated
436 within the basin.

437 On the γ^n = 26.0 isopycnal which bisects the layer exhibiting the rNPN anomaly at the
438 BATS station, the site sits surrounded by waters with a residual preNO$_3$ content of ~0 μM in the
439 annual climatology, with more distant waters exhibiting rNPN anomalies south of ~27 ºN and
440 waters with rPPN anomalies north of ~37 ºN (Fig. S7). Plots of residual preNO$_3$ versus CFC-11
441 and CFC-12 age on γ^n = 26.0 again reveal essentially no residual preNO$_3$ gradient with
442 increasing age (Fig. S7). Given the lack of a residual preNO$_3$ tracer gradient with water mass age
443 and the observation of a repeating seasonal pattern of rNPN anomaly formation at the BATS
444 station on γ^n = 26.0 (Fig. 2), we conclude that lateral advective mixing cannot explain the
445 observed seasonal rNPN anomalies, instead suggestive of biological mechanisms supporting
446 rNPN anomaly formation at the BATS station.

447 Examination of the residual preNO$_3$ tracer on the γ^n = 25.4 density surface (the surface
448 approximately bisecting the 200 – 250 m layer near ALOHA) in the North Pacific within the
449 World Ocean Atlas climatology reveals that Station ALOHA sits near the southern boundary of
450 waters with a residual preNO$_3$ content of 0 – 1.5 μM that extends as far north as 40 ºN and as far
451 east as 130 ºW (Fig. S8). Waters with higher residual preNO$_3$ content of 2 – 4 μM are located to
452 the south of Station ALOHA, beginning around the vicinity of the big island of Hawaii (Fig. S8).
453 Examination of plots of residual preNO$_3$ versus CFC-11 and CFC-12 age on γ^n = 25.4 in the
454 North Pacific reveals that Station ALOHA lies between younger, low residual preNO$_3$ content
455 waters to the north with older, higher residual preNO$_3$ content waters to the south (Fig. S8).
456 Mixing of these waters along γ^n = 25.4 may explain the observed ~1 μM residual preNO$_3$

concentration present at 200 – 250 m depth in Figure 1. This feature is noticeably absent at BATS, (Figure S6) consistent with a minor role for advective mixing there.

On the $\gamma^n = 24.7$ isopycnal which bisects the density layer exhibiting the rNPN anomaly at Station ALOHA, the site is surrounded by waters with rNPN anomalies on the order of –1 – 0 μM (Fig. S9). Plots of residual $preNO_3$ versus CFC-11 and CFC-12 age on $\gamma^n = 24.7$ reveal essentially no residual $preNO_3$ age gradient (Fig. S9). Similar to the BATS station, given the lack of a residual $preNO_3$ age gradient on $\gamma^n = 24.7$ and the observation of seasonal formation of rNPN anomalies, we conclude that lateral advective mixing cannot explain the observed rNPN anomalies, suggestive of biological mechanisms.

Biological mechanisms

Lateral mixing may explain the observed rPPN anomaly below ~200 m at Station ALOHA: however, the euphotic zone rPPN anomalies and subsurface rNPN anomalies at each site are generated by a local biological mechanism. Biological formation of rNPN anomalies requires either O_2 consumption without concomitant stoichiometric nitrate accumulation or nitrate drawdown without concomitant stoichiometric O_2 production. Formation of rPPN anomalies requires either O_2 production without concomitant stoichiometric nitrate drawdown or nitrate accumulation without concomitant stoichiometric O_2 consumption. Having accounted for the non-Redfield $-O_2$:N DOM remineralization stoichiometry at each site (see Table 2 for the rate of NPN/PPN anomaly formation attributable to N-poor DOM remineralization), we hypothesize three other biological mechanisms to explain the observed seasonal formation rates and integrated quantities of concurrent rPPN accumulation in the euphotic zone and rNPN accumulation in the subsurface at the ALOHA and BATS stations: 1) biological production, export, and remineralization of N-deficient transparent exopolymer particles (TEP); 2)

heterotrophic bacterial uptake of nitrate to remineralize N-poor organic matter; 3) vertical migration of autotrophic phytoplankton down to the nutricline to acquire nitrate with subsequent photosynthetic oxygen production within the euphotic zone.

TEP – Transparent exopolymer particles (TEP) are the polysaccharide-rich exudate of phytoplankton that accumulate in the size range <1 to >100 μm in aquatic systems (Mari et al., 2017). TEP is both sticky and positively buoyant in seawater (Azetsu-Scotte and Passow, 2004), leading to aggregation and flotation towards the surface, with large enrichments of TEP present in the sea surface microlayer (Wurl et al., 2009). Being comprised of nearly pure saccharide material, TEP is a carbon rich and essentially N-deficient pool of non-sinking particulate organic carbon formed within the euphotic zone of marine systems by phytoplankton production (Alldredge et al., 1993). TEP production has been hypothesized to contribute to "carbon overconsumption" in low nutrient oligotrophic marine ecosystems (Toggweiler, 1993) where organic matter is produced in non-Redfield, C-rich/N-poor proportions. Due to its positive buoyancy (Mari et al., 2017), TEP has been viewed as a non-contributor to upper ocean carbon export; however, some portion of the TEP pool is associated with sufficient ballasting particles (e.g. clays, biogenic minerals) to achieve negative buoyancy, and may comprise a slowly sinking (a few meters per year) pool of organic carbon exported below the euphotic zone (Mari et al., 2017). TEP production and remineralization stoichiometry has the correct sense; O_2 production without Redfieldian nitrate drawdown within the euphotic zone, O_2 consumption without Redfieldian nitrate accumulation within the mesopelagic, to contribute to both the observed rPPN anomalies within the euphotic zone and rNPN anomalies in the upper mesopelagic at the ALOHA and BATS stations in our analysis.

We use field data of TEP concentrations near the BATS and ALOHA stations and a few simplifying assumptions to test for the importance of this process as a contributor to the dual rNPN/rPPN anomalies. Our estimates of the potential for TEP cycling to contribute to the observed euphotic zone rPPN and subsurface rNPN anomaly formation rates assume 1) that TEP is pure carbohydrate (CH_2O); without any N content, such that TEP production/remineralization C:O_2 stoichiometry can be assumed 1:1 (e.g. $CO_2 + H_2O \Leftrightarrow CH_2O + O_2$), and 2) that there exists a sufficiently large and dense TEP pool to sink rapidly enough to contribute to annual carbon export and O_2 remineralization budgets. Both assumptions, if incorrect, will overestimate the TEP contribution. In conjunction with TEP cycling, Coomassie stainable particles are transparent protein-containing particles (Long and Azam, 1996) that can reach similar concentrations within the oligotrophic euphotic zone as TEP (Cisternas-Novoa et al., 2015). Thus, the assumption that transparent exopolymer particle cycling delivers only C to the subsurface to drive rNPN anomaly formation may not be entirely valid. In addition, Mari et al. (2017) note that elevated TEP concentrations likely enhance material retention in the euphotic zone. Thus, our calculations that follow tend to maximize the contribution of TEP.

Cisternas-Novoa et al. (2015) measured TEP concentration depth profiles in the Sargasso Sea northeast of Bermuda on five separate occasions from February 2012 to June 2013. The profiles show a ~10 μg XG eq L^{-1} (xanthum gum equivalent) concentration excess between the upper 100 m and the 100-200 m layer (Fig. 15 in Cisternas-Novoa et al., 2015). We take this upper 100 m excess to represent the fraction of the euphotic zone TEP pool that is exported annually to the upper mesopelagic 100-200 m depth layer by a combination of physical sinking of a fraction of the TEP pool that becomes negatively buoyant or is delivered to the subsurface with wintertime vertical mixing. This assumption is supported by the observation that the

525 euphotic zone to mesopelagic TEP concentration gradient is nearly erased in the winter profile,
526 presumably due to wintertime convective mixing, and reappears following the spring bloom,
527 remaining relatively unchanged throughout the late spring/summer month profiles. TEP in
528 xanthum gum equivalents can be converted to μg C L^{-1} units using a 0.63 conversion factor
529 (Engel, 2004) and again into μM units, yielding a Sargasso Sea upper ocean concentration excess
530 of ~0.5 μM TEP-C. Integrating over the surface to 80 m depth layer (the depth where rPPN
531 anomalies switch to rNPN anomalies), we obtain a potential TEP production and export flux of
532 42 mmol TEP-C m^{-2} yr^{-1} from the euphotic zone into the upper mesopelagic. Assuming 1:1 C:O_2
533 TEP production/remineralization stoichiometry, an O_2 production flux in the absence of nitrate
534 drawdown of 42 mmol O_2 m^{-2} yr^{-1} can be ascribed to TEP production within the euphotic zone,
535 and the same flux can be ascribed to O_2 consumption without concomitant nitrate accumulation
536 from TEP remineralization in the mesopelagic. We can convert this O_2 flux to a residual preNO_3
537 equivalent using Equation 1 and the values in Table 1, yielding estimates of 3.2 – 4.5 mmol N m^{-2}
538 yr^{-1} residual preNO_3 anomaly formation rate equivalents, depending on the choice of r_{POM}.
539 Thus, TEP formation within the euphotic zone of the Sargasso Sea has the potential to explain
540 5.2 – 5.4% of the estimated rPPN anomaly formation rate and 5.1 – 7.0% of the estimated rNPN
541 anomaly formation rate within the γ^n = 25.8 – 26.3 layer (Table 2).

542 The potential contribution of TEP cycling to rPPN/rNPN anomaly formation near the
543 BATS station can be also be estimated using published sinking rates for negatively buoyant TEP.
544 Again, using the TEP profiles from the Sargasso Sea from Cisternas-Novoa et al. (2015), we
545 estimate a concentration difference of ~5 μg XG eq L^{-1} between 100 m and 200 m depth (the
546 approximate depths exhibiting rNPN anomalies). Converting to molar carbon concentration
547 yields a quantity of ~0.26 μM TEP-C that is apparently remineralized within the rNPN anomaly

548 layer. We apply the TEP sinking rate of 0.04 d^{-1} from Hamanaka et al. (2002) to estimate the rate
549 of delivery of exported TEP from the euphotic zone into the upper mesopelagic, yielding a TEP
550 supply and remineralization flux of 10 μmol C m^{-3} d^{-1}. Depth and time integrated to 15 meters
551 and one year, i.e. the depth slowly sinking TEP will sink after one year, this flux becomes 56.9
552 mmol C m^{-2} yr^{-1} or O_2 units assuming 1:1 C:O_2 stoichiometry for TEP. Conversion of this O_2
553 flux into residual preNO_3 equivalents yields an estimated 4.3 – 6.0 mmol N m^{-2} yr^{-1} of the
554 observed rPPN/rNPN anomaly formation rate attributable to TEP cycling. Thus, computed using
555 the sinking rate, TEP formation within the euphotic zone has the potential to explain 7.0 – 7.3%
556 of the estimated rPPN anomaly formation rate and 6.9 – 9.3% of the estimated rNPN anomaly
557 formation rate within the γ^n = 25.8 – 26.3 layer.

558 Seasonal depth profiles of TEP concentration are unavailable for the subtropical North
559 Pacific near Station ALOHA. Wurl et al. (2011) measured TEP concentration profiles south of
560 the island of Hawaii during August/September 2009. We use the upper ocean concentration
561 excess present in these profiles with the TEP sinking rate of 0.04 d^{-1} to estimate the TEP cycling
562 contribution to rPPN/rNPN anomaly formation rates near Station ALOHA. The 100 to 200 m
563 concentration excess in TEP-C is ~1 μM yielding an export and supply flux of 40 μmol C m^{-3} d^{-1}
564 . Depth and time integrating for 15 m and one year, this flux becomes 220 mmol C m^{-2} yr^{-1}
565 (mmol O_2 m^{-2} yr^{-1}). Conversion of this O_2 flux to residual preNO_3 equivalents using equation 1
566 and values in Table 1, yields an estimated 16.2 – 21.8 mmol N m^{-2} yr^{-1} of the observed
567 rPPN/rNPN anomaly formation rate potentially attributable to TEP cycling at Station ALOHA.
568 Thus, TEP formation within the euphotic zone has the potential to explain 35.6 – 37.2% of the
569 estimated rPPN anomaly formation rate and 47.0 – 51.3% of the total estimated rNPN anomaly
570 formation rate within the combined γ^n = 24.2 – 25.2 layer (Table 2).

571 *Bacterial nitrate uptake* – Multiple studies have shown the uptake of nitrate and/or
572 phosphate by heterotrophic bacteria during the remineralization of organic matter or that
573 inorganic nutrients can limit bacterial OM consumption (e.g. Zweifel et al., 1993; Kirchman,
574 1994; Cotner et al., 1997; Rivkin and Anderson, 1997; Caron et al., 2000; Letscher et al., 2015).
575 Bacterial nitrate uptake to remineralize OM has the effect of creating an NPN anomaly (O_2
576 consumption without concomitant nitrate accumulation) and thus can only contribute to the
577 observed subsurface rNPN anomaly formation. It cannot contribute to either the formation of the
578 euphotic zone rPPN anomaly or surface mixed layer drawdown of DIC. If TEP cycling is an
579 important contributor to oligotrophic ocean C export and shallow subsurface O_2 consumption,
580 heterotrophic bacterial nitrate and/or phosphate uptake is a likely complementary biological
581 process, since the nutrient deficient content of TEP could require exogenous uptake of N and P
582 from the seawater media for bacterial production when growing on TEP organic matter. This
583 would result in an imbalance between rPPN and rNPN, in contrast to the results presented
584 earlier.

585 To assess the potential contribution of bacterial nitrate uptake to our observed rNPN
586 anomaly formation rates at the ALOHA and BATS stations, we examined the literature for
587 estimates of bacterial C production rates and bacterial biomass C:N ratios for the Sargasso Sea
588 and subtropical North Pacific. Carlson et al. (1996) measured bacterial production rates at the
589 BATS station using the ^{3}H-thymidine and ^{3}H-leucine uptake methods with average euphotic
590 zone rates of 23 pmol C L^{-1} d^{-1} by ^{3}H-thymidine and 0.41 nmol C L^{-1} d^{-1} by ^{3}H-leucine. Using a
591 bacterial biomass C:N of 5:1 for this region (Gunderson et al. 2002) and integrating for one year
592 and over the ~80 – 160 m thick layer exhibiting rNPN anomaly, yields an estimate of 0.17 – 3.0
593 mmol N m^{-2} yr^{-1} bacterial N demand. If we assume that bacteria satisfy *all* of their N demand via

uptake of seawater nitrate in this shallow subsurface layer, bacterial nitrate uptake can explain at most 0.5 – 3.5% of the estimated rNPN anomaly formation rate at the BATS station in the γ^n = 25.8 – 26.3 layer. This proposed mechanism still requires a process that removes bacterial N from the γ^n = 25.8 – 26.3 layer such that a rNPN anomaly is observed due to NO_3 uptake in the absence of stoichiometric O_2 accumulation. Diel vertically migrating grazers are a candidate mechanism whereby grazing on bacterial biomass and its eventual remineralization to NO_3 is spatially separated from respiration and O_2 consumption.

We can make a similar calculation for Station ALOHA using published ^{3}H-leucine bacterial production rate measurements (Church et al., 2004). The mean bacterial C production rate at 100 m is ~0.46 nmol C L^{-1} d^{-1}. Using the same bacterial biomass C:N of 5:1 and integrating for one year over the ~100 – 200 m thick layer exhibiting rNPN anomaly, yields an estimated 3.4 mmol N m^{-2} yr^{-1} bacterial N demand. If we again assume that bacteria satisfy *all* of their N demand from nitrate uptake, this process can explain at most 0 – 7% of the estimated rNPN anomaly formation rate at Station ALOHA in the combined γ^n = 24.2 – 25.2 layer.

Vertically migrating phytoplankton – From our analyses of the available published data, neither remineralization of N-poor DOM, TEP cycling, or heterotrophic bacterial nitrate uptake can quantitatively explain both the seasonal rPPN anomaly formation within the euphotic zone and subsurface rNPN anomaly formation observed at the ALOHA and BATS stations even with the generous assumptions made. Lastly, we examine the vertical migration of phytoplankton down to the nitracline as a potential biological mechanism to explain the dual rPPN/rNPN anomalies. The unique attributes of and evidence for vertical migration are briefly discussed here for background, as well as documentation of their presence in both oceans at or near the time-series stations. As a rare, giant component of the flora, net collections and *in-situ* observations by

617 divers constitute the bulk of observations, hence are somewhat out of the mainstream of current
618 phytoplankton observations.

619 Flagellate motility and cyanobacteria buoyancy control has been recognized for decades
620 as a strategy to exploit spatially disjunct light and nutrient fields (Cullen, 1985; Eppley et al.,
621 1968, Ganf and Oliver, 1982; Hasle, 1950; Steemann Nielsen, 1939) and was suggested for non-
622 flagellated marine species in *Pyrocystis* (Sukhanova and Rudyakov, 1973; Ballek and Swift,
623 1986; Rivkin et al., 1984). *Rhizosolenia* mats (macroscopic, multi-species (up to 7) associations
624 of *Rhizosolenia* spp.; Villareal and Carpenter, 1989) have been the model for understanding this
625 process (Villareal et al., 2014), with migration inferred for the diatoms *Ethmodiscus* spp. and
626 large *Rhizosolenia* spp., as well as the phycomate prasinophyte *Halosphaera* spp. in addition to
627 *Pyrocystis.* There is consistent evidence of high $\delta^{15}N$ composition of *Rhizosolenia* biomass
628 similar to sub-nutricline N (Villareal et al., 1993, Villareal et al., 2014), internal millimolar
629 nitrate pools that can only be acquired by direct uptake at μM concentrations (Villareal and
630 Lipschultz, 1995; Villareal et al., 1996; Woods and Villareal, 2008), buoyancy reversals linked
631 to nutrient status (Richardson et al., 1996), nitrate reductase activity (Joseph et al., 1997) induced
632 only when nitrate is the primary N source, ascent/descent rates of multiple m hr^{-1} (Villareal et al.,
633 2014; Moore and Villareal 1996), observation of *Rhizosolenia* mats from the surface to 305 m
634 (Pilskaln et al., 2005), and compositional difference in floating and sinking mats that mirror
635 physiological changes associated with nutrient depletion and carbohydrate ballasting (Villareal et
636 al., 1996). A key attribute in all giant phytoplankton migrators is the multiple m hr^{-1}
637 ascent/descent rates their large size (10^{7+} μm^3) permits (Moore and Villareal 1986). This allows
638 the required 50–100 m vertical excursions and when coupled with the large vacuole of these
639 giant phytoplankton, allow the necessary storage (mM concentrations in vacuoles that are 90+%

of total cell volume) for a multiple day migration and division cycle. Unlike the more widely known zooplankton vertical migration, open ocean phytoplankton migration is a multi-day cycle (Richardson et al., 1998; Villareal et al., 1996). It is asynchronous and not cued to diel rhythms as in coastal dinoflagellates or vertically migrating zooplankton.

Giant phytoplankton are found throughout the warmer oceans of the world and are specifically noted at both stations ALOHA and BATS (Figure S11-13). The required characteristics of buoyancy reversals, high internal nitrate pools and rapid ascent/descent have been found in multiple taxa from the Atlantic and Pacific Oceans (Villareal et al., 2014). The taxa *Halosphaera* (Villareal and Lipschultz, 1995), *Ethmodiscus* (Villareal and Lipschultz, 1995), *Rhizosolenia* (Villareal and Lipschultz, 1995), and *Pyrocystis* (Swift et al. 1973, Rivkin et al 1984, Villareal and Lipschultz 19965) occur in the Sargasso Sea and all exhibit positive buoyancy and have mM internal nitrate pools. In the Sargasso Sea, the non-motile dinoflagellate *Pyrocystis* has been the most extensively studied by E.J. Swift's lab in the 1980s. A 'once in a generation' migration cycle (Sukhanova and Rudyakov, 1973) was proposed for *Pyrocystis* based on differences in vegetative and reproductive cell maxima (~60 and 120 m, respectively). Vegetative stages were positively buoyant (up to 0.2 m h^{-1}; Kahn and Swift, 1978) while reproductive stages were negatively buoyant at up to 18 m h^{-1} in the Mona Passage, southwest N. Atlantic (Swift et al. 1976). In the Sargasso Sea, carbon budgets (Rivkin et al., 1984) and buoyancy changes upon nutrient depletion and addition (Ballek et al., 1986) all supported a vertical migration life cycle. In single-cell analysis from field material collected off Bermuda, *Pyrocystis* internal nitrate concentrations ranged from 0-8 mM with floating cells containing significantly higher concentrations (p=0.05) than sinking cells (Villareal and Lipschultz, 1995). Such elevated internal nitrate can only be acquired at μM nitrate concentrations found in the

663 nutricline. Abundance maxima in the upper ~200 m of the Sargasso Sea/southwest N. Atlantic
664 range from 100-200 cells m^{-3}, with typical values reported of 18-75 cells m^{-3} (Rivkin et al.,
665 1984), 10-50 cells m^{-3} (Ballek and Swift, 1986) and 10-30 cells m^{-3} (Swift et al., 1981). While
666 the other migrating taxa are found in the Sargasso Sea near Bermuda, there is no data on
667 abundance in the N. Atlantic other than for *Ethmodiscus*. *Ethmodiscus* was found at every station
668 sampled on three cruises in the southwest N. Atlantic (n=18, ~17-25°N, 66-77°W) with
669 abundance ranging from 0.03-4.7 cells m^{-3}. Free-living chains of *Rhizosolenia* were routinely
670 isolated by hand-collection with SCUBA at Bermuda (Moore and Villareal, 1996a,b; Richardson
671 et al., 1996) and were widely noted by Carpenter et al. (1977) in the Caribbean. Cleve (1900)
672 reported *R. castracanei* (a giant, migrating diatom found both free-living and in *Rhizosolenia*
673 mats) to occur in the Sargasso Sea as well as the tropical Atlantic, Caribbean Sea, Florida current
674 to Newfoundland Banks, and the Azores.
675 In the Pacific, the range of *Ethmodiscus*, *Pyrocystis*, and *Rhizosolenia* mats includes the
676 study site at Station ALOHA (Figures S11-13). Unlike the Atlantic where mats are generally
677 very rare (~0.001 mats m^{-3}, Carpenter et al., 1977), *Rhizosolenia* mats dominate in the Pacific.
678 Abundance ranges up to several hundred mats m^{-3}, depending on the mat size and enumeration
679 methods (Villareal et al., 1996, Villareal et al., 1999; Villareal et al., 2014). Quantitative net
680 surveys of *Ethmodiscus* north of Hawaii yielded abundance ranges of $<0.1 - >2$ cells m^{-3}
681 (Villareal et al., 2007). Both *Halosphaera* and *Pyrocystis* were present, but not quantified.
682 Further to the west, Soviet-era literature documents *Pyrocystis* at 10-50 cells m^{-3} in the upper 200
683 m (Sukhanova and Rudyakov, 1973; Sukahova, 1973). Free-living giant *Rhizosolenia* were
684 observed by divers at all stations sampled in the N. Pacific (Villareal, unpubl. obs.), and
685 overlapped 100% with *Rhizosolenia* mats (Fig. 2 in Villareal et al., 2014); *R. castracanei* was

reported across the Pacific Ocean (Fig. 8 in Semina and Levashova, 1977). It should be noted that net collections disrupt *Rhizosolenia* mats (Alldredge and Silver, 1982) and the large diameter species such as *R. castracanei* in the mats will appear as free-chains and cells in the literature.

For rNPN and rPPN development, the unique characteristics of vertical migration are that cells acquire and store nitrate at depth, transport it into the euphotic zone, and then reduce it internally to biomass concomitant with oxygenic photosynthesis. Nitrate transport calculations by vertical migration have a number of assumptions and caveats including variability in abundance, particularly for *Halosphaera* spp. (Villareal et al., 2014). However, site-specific estimates in the Pacific north of Station ALOHA yielded rates of 6–444 μmol N m^{-2} d^{-1} for *Rhizosolenia* mats. Four other taxa yielded transport rates of 3.2 (*Ethmodiscus* spp.), 9.2 (free living *Rhizosolenia* spp.), 17.0 (*Pyrocystis* spp.) and 33.2 (*Halosphaera* spp.) μmol N m^{-2} d^{-1}. These taxa exhibit basin-specific abundance patterns (i.e. *Rhizosolenia* mats are rare in the N. Atlantic; Carpenter et al., 1977, *Halosphaera viridis* has an extensive subsurface presence in the deep Mediterranean in winter (Wiebe et al., 1974); however, it is clear that the generalized rates are consistent with both the known abundance and distribution data as well as the required rNPN and rPPN rates at both the BATS station (126 – 239 and 169 – 225 μmol N m^{-2} d^{-1}, respectively) and Station ALOHA (88 – 122 and 119 – 168 μmol N m^{-2} d^{-1}, respectively). There are several implications of this. Lower abundance or turnover times of this flora will still have substantial effects on rNPN and rPPN. Patchiness in abundance (Villareal, 2007; et al., 2014) or concentration of buoyant particles by mesoscale fronts (Guidi, 2012) could lead to significant local perturbations on rNPN and rPPN.

We estimate the potential contribution of vertically migrating phytoplankton to the rNPN and rPPN anomaly features at the two stations by subtracting our estimates of the contributions of TEP cycling and bacterial nitrate uptake to rNPN and/or rPPN formation from the total observed rNPN/rPPN anomaly formation rates (presented in Table 2). By difference, phytoplankton vertical migration potentially explains 16 – 21 mmol N m^{-2} yr^{-1} or 45 – 50% of rNPN anomaly formation and 27 – 36 mmol N m^{-2} yr^{-1} or 59 – 62% of rPPN anomaly formation at Station ALOHA (Table 2). At the BATS station, phytoplankton vertical migration potentially explains 43 – 78 mmol N m^{-2} yr^{-1} or 90 – 93% of rNPN anomaly formation and 59 – 76 mmol N m^{-2} yr^{-1} or 87 – 95% of rPPN anomaly formation. These are likely underestimates because the bacterial nitrate uptake and TEP contribution are maximum estimates.

Contributions to carbon and phosphorus budgets

DIC – Vertically migrating phytoplankton can also help explain the observed summertime DIC drawdown (Gruber et al., 1998; Keeling et al., 2004) in the absence of measurable nitrate from the mixed layer at both the ALOHA and BATS stations. The concurrently operating migration cycles of different individuals would continually bring intracellular nitrate-rich migrators into the surface mixed layer where their oxygenic photosynthesis would draw down DIC and release dissolved O_2, contributing to rPPN anomaly formation within the mixed layer. High intracellular nitrate gradients within migrators (mM to nM across cell membranes) can also lead to excretion of dissolved nitrate into the water column (Singler and Villareal, 2005). Thus, nitrate leakage from migrators could help explain the observation of a presumed subsurface nitrate source supporting pico-eukaryotic phytoplankton in the mixed layer, even during the stratified summer months at the BATS station (Fawcett et al.,

731 2011). However, nitrogen derived from migrator-mediated nitrate excretion is required to sink
732 out of the mixed layer in some form in order to contribute to summertime net DIC drawdown at
733 these two sites. Regardless of how nitrate is acquired and internally reduced (by migrators or by
734 release and uptake by non-migrating phytoplankton), it will contribute to the observed rPPN.
735 We can compare our estimated rates of rPPN formation within the euphotic zone with the
736 summertime mixed layer DIC drawdown at each time-series site using assumptions on the
737 appropriate O_2:C:N stoichiometry of production. Although seasonal rPPN formation exhibits the
738 largest increase in preNO_3 concentrations at ~50 – 100 m depth, seasonal accumulation of
739 positive residual preNO_3 is observed within the mixed layer (~0 – 30 m) at both sites (Fig. 1, 2).
740 At Station ALOHA, net community production during the six-month summer to fall
741 period represents ~40% of the 2.3 mol C m^{-2} yr^{-1} ANCP (Keeling et al., 2004), yielding a
742 summertime mixed layer DIC drawdown of ~920 mmol C m^{-2}. Our estimated rate of euphotic
743 zone rPPN formation during this same seasonal period is 33 – 81 mmol N m^{-2} (Table 1). The
744 summertime DIC drawdown can be converted to residual preNO_3 nitrogen equivalents using the
745 literature range in O_2:C stoichiometries of production of 1.0 – 1.6 (Paulmier et al., 2009), and the
746 DOM and POM weighted O_2:N stoichiometries of production (using the values in Table 1)
747 yielding values of 7.8 – 14.3 for the C:N of summertime new production at Station ALOHA.
748 Summertime DIC drawdown converted to preNO_3 equivalents is 64 – 118 mmol N m^{-2}. Thus,
749 rPPN formation within the euphotic zone can potentially explain 28 – >100% of the mixed layer
750 DIC drawdown at Station ALOHA.
751 The estimated rate of euphotic zone rPPN formation during summer-to-fall at the BATS
752 station is 50 – 96 mmol N m^{-2} (Table 1). Net community production during this seasonal period
753 is ~45% of the 2.3 mol C m^{-2} yr^{-1} ANCP (Gruber et al., 1998), yielding a summertime mixed

754 layer DIC drawdown of ~1035 mmol C m^{-2}. Conversion of the summertime DIC drawdown to
755 preNO_3 nitrogen equivalents following a similar approach as our calculation at Station ALOHA
756 uses a DOM and POM weighted C:N of 7.9 – 14.8 for summertime new production at the BATS
757 station, yielding 70 – 131 mmol N m^{-2}. Thus, rPPN formation within the euphotic zone can
758 potentially explain 38 – >100% of the mixed layer DIC drawdown at the BATS station.
759 *prePO_4* – We also investigated for the presence of subsurface residual negative prePO_4
760 anomalies at the ALOHA and BATS stations. Station ALOHA does not exhibit a subsurface
761 residual negative prePO_4 anomaly (Fig. 3), with the exception of a small anomaly present in
762 years 2002 – 2004. There does exist a subsurface residual negative prePO_4 anomaly and euphotic
763 zone residual positive prePO_4 anomaly at the BATS station (Fig. 4), present throughout the time
764 series and monthly averaged climatology that is coincident in both seasonal timing and
765 depth/density layer location as the rNPN and rPPN anomalies (Fig. 2). Carbon to phosphorus
766 ratios exhibit their global maxima in the subtropical North Atlantic for phytoplankton biomass
767 (Martiny et al., 2013), dissolved organic matter (Letscher and Moore, 2015), and exported
768 organic matter (Teng et al., 2014). The hypothesized phosphorus limitation of this basin
769 (Ammerman et al., 2003; Moore et al., 2004) may explain the contrasting observations of the
770 presence of a residual negative prePO_4 anomaly at the BATS station in the North Atlantic while
771 not at Station ALOHA in the North Pacific. Because of the many observations of elevated C:P
772 across organic matter pools in the North Atlantic, we tested for the theoretical value of $R_{-O2:P}$, the
773 stoichiometric ratio of O_2 consumed to phosphate released during the remineralization of organic
774 matter, needed to eliminate the subsurface residual negative prePO_4 anomaly at the BATS
775 station. This theoretical value of $R_{-O2:P}$ was found to be ~1000:1 (Fig. S10), which is ~4x higher

776 than the inferred $R_{-O2:P}$ for the North Atlantic from an inversion of subsurface O_2 and phosphate
777 data (DeVries and Deutsch, 2014).

778 We hypothesize that P-limited or P-stressed vertically migrating phytoplankton also take
779 up phosphate at the nutricline in combination with nitrate to contribute to both the observed
780 rNPN/rPPN and the subsurface residual negative $prePO_4$ anomaly present at the BATS station.
781 Limited sampling in the waters between Hawaii and California indicated N:P ratios were not
782 significantly different between sinking and ascending *Rhizosolenia* mats (N:P ~26-30) while C:P
783 ratios were significantly different ($p = 0.05$, C:P sinkers = 388 ± 66; C:P ascending = 221 ± 43).
784 This is consistent with simultaneous uptake of N and P at depth, but carbon consumption at
785 depth relative to the surface. Further data on phosphate composition of vertically migrating
786 phytoplankton are needed to confirm our hypothesis.

787

788 **Concluding Remarks**

789 Subsurface residual $preNO_3$ anomalies cover a large portion of the subtropical ocean
790 (Fig. 5). Our analyses have confirmed and emphasized that the Abell et al. (2005) use of non-
791 Redfield DOM stoichiometry in the calculation of $preNO_3$ is required, and an explicit derivation
792 of r_{DOM} is needed. The residual $preNO_3$ calculation revealed a subsurface rNPN anomaly that is
793 not accounted for by organic material remineralization. Our consideration of three possible
794 contributing biological mechanisms suggest that the dominant role (in decreasing order of
795 importance) is played by vertically migrating giant phytoplankton, TEP
796 formation/remineralization, and bacterial utilization of nitrate (Table 2). The analyses also
797 revealed a near-surface rPPN anomaly that is approximately balanced and concurrent with the
798 rNPN anomaly. This feature is coherent with the subsurface oxygen maximum (SOM) and we

799 interpret this as evidence that the "missing" nitrate from the rNPN anomaly is mechanistically
800 linked to the SOM. The seasonal euphotic zone rPPN anomaly can also explain a significant
801 fraction of the unexplained summertime drawdown of DIC from the mixed layer at both sites.
802 Whether this phenomenon is predominately carried out by TEP production and export, vertically
803 migrating phytoplankton, or a combination of both awaits future direct field observations.
804 Fraga (2001) developed an independent assessment of the impact of vertical migration on
805 the NO tracer (functionally related to our residual preNO_3 tracer) based on first principles of
806 photosynthetic production and biosynthesis of biomass. For ecosystems containing both coastal
807 dinoflagellates and oceanic diatoms, a subsurface minimum in NO and a related tracer, NCO
808 (NO corrected for the stoichiometry of carbohydrate synthesis) formed. For migrating
809 *Rhizosolenia*, the NO and NCO minimum was at ~150 m with negative anomalies from ~80 to
810 ~200 m (Fig. 6 in Fraga, 2001). The Fraga (2001) formulation also included an explicit term for
811 release of soluble carbohydrate (functionally equivalent to TEP). Migrating phytoplankton can
812 clearly provide a mechanistic linkage via upward nutrient transport to the observed NO
813 anomalies.
814 More observations of upper ocean, surface to ~200 m, abundance estimates of the
815 vertically migrating phytoplankton taxa, their intracellular nitrate and phosphate contents, and
816 their migration timescales are needed to confirm the hypothesis by multiple authors (e.g. Cullen,
817 1985; Richardson et al., 1998; Fraga, 2001; Villareal et al., 2014) of this flora's important role in
818 nutrient transport and rNPN/rPPN anomaly formation at the time-series stations (this study).
819 Given the circumglobal, warm-water range of this oligotrophic flora (Fig. S11-S13), it is
820 reasonable to expect upward nutrient transport throughout the subtropical gyres. TEP may
821 contribute as well, depending on the stoichiometry of production/remineralization and shifts in

822 buoyancy characteristics. More information on the mass quantities of the positively and
823 negatively buoyant TEP within the euphotic zone and its C:N content is needed to better
824 constrain the role of this mechanism in rPPN/rNPN anomaly formation in the subtropics. In
825 addition, *Rhizosolenia* mats are embedded in a TEP matrix (Pilskaln et al., 2005), so it is likely
826 that all three biological mechanisms we investigated are non-mutually exclusive with vertically
827 migrating phytoplankton contributing to TEP production/export, nitrate transport across the
828 nitracline into the euphotic zone, and bacterial nitrate uptake to remineralize N-deficient TEP.
829 While phytoplankton TEP production appears to be favored in the upper water column,
830 positively buoyant TEP production/formation in the nutricline could also serve to provide a
831 means for transporting entrained particulates upward into the euphotic zone. Both migration and
832 TEP are difficult to measure and the challenge will be to develop methods and time-series to
833 record these biologically driven processes at the requisite time and space scales.
834
835
836
837 **Acknowledgements**
838 RTL thanks the efforts of the scientists, crew, and staff that have supported the Hawaiian Ocean
839 Time Series and Bermuda Atlantic Time Series for nearly thirty years, including the continuing
840 financial support of the National Science Foundation Biological and Chemical Oceanography
841 Programs. TAV acknowledges support from NSF OCE 1537546 and wishes to thank all the
842 students, graduate and undergraduate, that provided the diving support essential to this work as
843 well as the officers and crew of the research vessels involved in this work.
844

References

Abell, J., Emerson, S., and Keil, R. G.: Using preformed nitrate to infer decadal changes in DOM remineralization in the subtropical North Pacific, Global biogeochemical cycles, 19(1), 2005.

Abell, J., Emerson, S., and Renaud, P.: Distributions of TOP, TON and TOC in the North Pacific subtropical gyre: Implications for nutrient supply in the surface ocean and remineralization in the upper thermocline, Journal of Marine Research, 58(2), 203-222, 2000.

Alldredge, A. L., Passow, U., and Logan, B. E.: The abundance and significance of a class of large, transparent organic particles in the ocean, Deep Sea Research Part I: Oceanographic Research Papers, 40(6), 1131-1140, 1993.

Alldredge, A. L., and Silver, M. W.: Abundance and production rates of floating diatom mats (*Rhizosolenia castracanei* and *Rhizosolenia imbricata* var. *shrubsolei*) in the eastern Pacific Ocean., Mar. Biol., 66, 83-88, 1982.

Ammerman, J. W., Hood, R. R., Case, D. A., and Cotner, J. B.: Phosphorus deficiency in the Atlantic: An emerging paradigm in oceanography, Eos, Transactions American Geophysical Union, 84(18), 165-170, 2003.

Anderson, L. A.: On the hydrogen and oxygen content of marine phytoplankton, Deep Sea Research Part 1: Oceanographic Research Papers, 42(9), 1675-1680, 1995.

Anderson, L. A., and Sarmiento, J. L.: Redfield ratios of remineralization determined by nutrient data analysis, Global biogeochemical cycles, 8(1), 65-80, 1994.

Azetsu-Scott, K., and Passow, U.: Ascending marine particles: Significance of transparent exopolymer particles (TEP) in the upper ocean, Limnol. Oceanogr., 49, 741-748, 2004.

Ballek, R. W., and Swift, E.: Nutrient-and light-mediated buoyancy control of the oceanic non-motile dinoflagellate *Pyrocystis noctiluca* Murray ex Haeckel (1890), Journal of Experimental Marine Biology and Ecology, 101(1-2), 175-192, 1986.

Bauerfeind, E.: Primary production and phytoplankton biomass in the equatorial region of the Atlantic at 22° west, Oceanological Acta, Proceedings of the International Symposium on Equatorial Vertical Motion, 131-136, 1987.

Belyayeva, T. V.: Abundance of *Ethmodiscus* in Pacific plankton, Oceanology, Academy of Science, USSR, 10, 672-675 (Translation by the American Geophysical Union), 1970.

Belyayeva, T. V.: Range and numbers of diatoms in the genus *Ethmodiscus* Castr. in the Pacific plankton and sediments, Oceanology, Academy of Science, USSR, 8, 79-85, (Translation by the American Geophysical Union), 1968.

Booth, B. C.: Vernal phytoplankton community in the eastern subarctic Pacific: Predominant species, in: Sixth International Symposium on Fossil and Living Diatoms, edited by: Simonsen, R., 339-358, 1980.

Broecker, W. S.: "NO" A conservative water-mass tracer, Earth Planet. Sci. Lett., 23, 100-107, 1974.

Carlson, C. A., Ducklow, H. W., and Sleeter, T. D.: Stocks and dynamics of bacterioplankton in the northwestern Sargasso Sea, Deep Sea Research Part II: Topical Studies in Oceanography, 43(2-3), 491-515, 1996.

Caron, D. A., Lim, E. L., Sanders, R. W., Dennett, M. R., and Berninger, U. G.: Responses of bacterioplankton and phytoplankton to organic carbon and inorganic nutrient addition in two oceanic ecosystems, Aquatic Microbial Ecology, 22, 175-184, 2000.

Carpenter, E. J., Harbison, R. G., Madin, L. P., Swanberg, N. R., Biggs, D. C., Hulburt, E. M., McAlister, V. L., and McCarthy, J. J.: *Rhizosolenia* Mats, Limnol. Oceanogr., 22, 739-741, 1977.

Church, M. J., Ducklow, H. W., and Karl, D. M.: Light dependence of [3H] leucine incorporation in the oligotrophic North Pacific Ocean, Applied and Environmental Microbiology, 70(7), 4079-4087, 2004.

Cisternas-Novoa, C., Lee, C., and Engel, A.: Transparent exopolymer particles (TEP) and Coomassie stainable particles (CSP): Differences between their origin and vertical distributions in the ocean, Marine Chemistry, 175, 56-71, 2015.

Cleve, P.: Seasonal distribution of Atlantic plankton organisms., D. R. Bonniers, Göteborg, 1900.

Cotner, J. B., Ammerman, J. W., Peele, E. R., and Bentzen, E.: Phosphorus-limited bacterioplankton growth in the Sargasso Sea, Aquatic Microbial Ecology, 13(2), 141-149, 1997.

Cowen, J. P., and Holloway, C. F.: Structural and chemical analysis of marine aggregates: in-situ macrophotography and laser confocal and electron microscopy, Marine Biology (Berlin), 126, 163-174, 1996.

Cullen, J. J.: Diel vertical migration by dinoflagellates: roles of carbohydrate metabolism and behavioral flexibility, in: Migration: mechanisms and adaptive significance, edited by: Rankin, M. A., Marine Science Institute, Port Aransas, 135-152, 1985.

Darwin, C.: The Voyage of the Beagle, Natural History Library edition (1962), edited by: Engle, L., Doubleday, New York, 524 pp., 1860.

DeVries, T., and Deutsch, C.: Large-scale variations in the stoichiometry of marine organic matter respiration, Nature Geoscience, 7(12), 890, 2014.

Doney, S. C. and Bullister, J. L.: A chlorofluorocarbon section in the eastern North Atlantic, Deep Sea Research I, 39(11-12A), 1857-1883, 1992.

Emerson, S.: Annual net community production and the biological carbon flux in the ocean, Global Biogeochemical Cycles, 28(1), 14-28, 2014.

Emerson, S., Quay, P., Karl, D., Winn, C., Tupas, L., and Landry, M.: Experimental determination of the organic carbon flux from open-ocean surface waters, Nature, 389(6654), 951, 1997.

Engel, A.: Distribution of transparent exopolymer particles (TEP) in the northeast Atlantic Ocean and their potential significance for aggregation processes, Deep Sea Research Part I: Oceanographic Research Papers, 51(1), 83-92, 2004.

Eppley, R. W., Holm-Hansen, O., and Strickland, J. D. H.: Some observations on the vertical migration of dinoflagellates, J. Phycol., 4, 333-340, 1968.

Fawcett, S. E., Lomas, M. W., Casey, J. R., Ward, B. B., and Sigman, D. M.: Assimilation of upwelled nitrate by small eukaryotes in the Sargasso Sea, Nature Geoscience, 4(10), 717, 2011.

Fraga, F.: Phytoplanktonic biomass synthesis: application to deviations from Redfield stoichiometry, Sci. Mar., 65, 153-169, 2001.

Fraga, F., Pérez, F. F., Figueiras, F. G., and Rios, A. F.: Stoichiometric variations of N, P, C and O_2 during a *Gymnodinium catenatum* red tide and their interpretation, Mar. Ecol. Prog. Ser., 87, 123-134, 1992.

Fraga, F., Rios, A. F., Pérez, F. F., Estrada, M., and Marrase, C.: Effect of upwelling pulses on excess carbohydrate synthesis as deduced from nutrient, carbon dioxide, and oxygen profiles, Mar. Ecol. Prog. Ser., 189, 65-75, 1999.

Ganf, G. G., and Oliver, R. L.: Vertical separation of light and available nutrients as a factor causing replacement of green algae by blue-green algae in the plankton of a stratified lake, The Journal of Ecology, 829-844, 1982.

Garcia, H. E., Locarnini, R. A., Boyer, T. P., Antonov, J. I., Baranova, O. K., Zweng, M. M., Reagan, J. R., Johnson, D. R.: World Ocean Atlas 2013, Volume 3: Dissolved Oxygen, Apparent Oxygen Utilization, and Oxygen Saturation, S. Levitus, Ed., A. Mishonov Technical Ed., NOAA Atlas NESDIS 75, 27, 2014a.

Garcia, H. E., Locarnini, R. A., Boyer, T. P., Antonov, J. I., Baranova, O. K., Zweng, M. M., Reagan, J. R., Johnson, D. R.: World Ocean Atlas 2013, Volume 4: Dissolved Inorganic Nutrients (phosphate, nitrate, silicate), S. Levitus, Ed., A. Mishonov Technical Ed., NOAA Atlas NESDIS 76, 25, 2014b.

Goncalves da Silva, M. G.: Diatom (Bacillariophyceae) distribution in the continental shelf of Pernambuco (Brazil).), Trab. Oceanogr. Univ. Fed. Pernambuco., 17, 7-46 (in Spanish), 1982.

Gruber, N., Keeling, C. D., and Bates, N. R.: Interannual variability in the North Atlantic Ocean carbon sink, Science, 298(5602), 2374-2378, 2002.

Gruber, N., Keeling, C. D., and Stocker, T. F.: Carbon-13 constraints on the seasonal inorganic carbon budget at the BATS site in the northwestern Sargasso Sea, Deep Sea Research Part I: Oceanographic Research Papers, 45(4-5), 673-717, 1998.

Guidi, L., Calil, P. H. R., Duhamel, S., Bjoerkman, K. M., Doney, S. C., Jackson, G. A., Li, B., Church, M. J., Tozzi, S., Kolber, Z. S., Richards, K. J., Fong, A. A., Letelier, R. M., Gorsky, G., Stemmann, L., and Karl, D. M.: Does eddy-eddy interaction control surface phytoplankton distribution and carbon export in the North Pacific Subtropical Gyre?, J. Geophys. Res.-Biogeosci., 117, 10.1029/2012jg001984, 2012.

Gundersen, K., Heldal, M., Norland, S., Purdie, D. A., and Knap, A. H.: Elemental C, N, and P cell content of individual bacteria collected at the Bermuda Atlantic Time-series Study (BATS) site, Limnology and Oceanography, 47(5), 1525-1530, 2002.

Hamanaka, J., Tanoue, E., Hama, T., and Handa, N.: Production and export of particulate fatty acids, carbohydrates and combined amino acids in the euphotic zone, Marine Chemistry, 77(1), 55-69, 2002.

Hansell, D. A., and Carlson, C. A.: Biogeochemistry of total organic carbon and nitrogen in the Sargasso Sea: control by convective overturn, Deep Sea Research Part II: Topical Studies in Oceanography, 48(8), 1649-1667, 2001.

Hasle, G. R.: Phototactic vertical migration in marine dinoflagellates, Oikos, 2(2), 162-175, 1950.

Jenkins, W. J., and Doney, S. C.: The subtropical nutrient spiral, Global Biogeochemical Cycles, 17(4), 2003.

Jenkins, W. J., and Goldman, J. C.: Seasonal oxygen cycling and primary production in the Sargasso Sea, Journal of Marine Research, 43(2), 465-491, 1985.

Johnson, K. S., Riser, S. C., and Karl, D. M.: Nitrate supply from deep to near-surface waters of the North Pacific subtropical gyre, Nature, 465(7301), 1062, 2010.

Joseph, L., Villareal, T. A., and Lipschultz, F.: A high sensitivity nitrate reductase assay and its application to vertically migrating Rhizosolenia mats, Aquatic Microbial Ecology, 12(1), 95-104, 1997.

Kahn, H., and Swift, E.: Positive buoyancy through ionic control in the nonmotile marine dinoflagellate *Pyrocystis noctiluca* Murray ex Schuett, Limnology and Oceanography, 23, 649-658, 1978.

Keeling, C. D., Brix, H., and Gruber, N.: Seasonal and long-term dynamics of the upper ocean carbon cycle at Station ALOHA near Hawaii, Global Biogeochemical Cycles, 18(4), 2004.

Kirchman, D. L.: The uptake of inorganic nutrients by heterotrophic bacteria, Microbial Ecology, 28(2), 255-271, 1994.

Letscher, R. T., Knapp, A. N., James, A. K., Carlson, C. A., Santoro, A. E., and Hansell, D. A.: Microbial community composition and nitrogen availability influence DOC remineralization in the South Pacific Gyre, Marine Chemistry, 177, 325-334, 2015.

Letscher, R. T., and Moore, J. K.: Preferential remineralization of dissolved organic phosphorus and non-Redfield DOM dynamics in the global ocean: Impacts on marine productivity, nitrogen fixation, and carbon export, Global Biogeochemical Cycles, 29(3), 325-340, 2015.

Letscher, R. T., Primeau, F., and Moore, J. K.: Nutrient budgets in the subtropical ocean gyres dominated by lateral transport, Nature Geoscience, 9(11), 815-819, 2016.

Long, R. A., and Azam, F.: Abundant protein-containing particles in the sea, Aquatic Microbial Ecology, 10, 213, 1996.

Mari, X., Passow, U., Migon, C., Burd, A. B., and Legendre, L.: Transparent exopolymer particles: Effects on carbon cycling in the ocean, Progress in Oceanography, 151, 13-37, 2017.

Martin, J. H., Knauer, G. A., Karl, D. M., and Broenkow, W. W.: VERTEX: carbon cycling in the northeast Pacific. Deep Sea Research Part A, Oceanographic Research Papers, 34(2), 267-285, 1987.

Martinez, L. A.: Nitrogen fixation by floating diatom mats: a source of new nitrogen to oligotrophic ocean waters, Biology, University of California, Santa Cruz, 23 pp., 1982.

Martiny, A. C., Pham, C. T., Primeau, F. W., Vrugt, J. A., Moore, J. K., Levin, S. A., and Lomas, M. W.: Strong latitudinal patterns in the elemental ratios of marine plankton and organic matter, Nature Geoscience, 6(4), 279, 2013.

Michaels, A. F., Bates, N. R., Buesseler, K. O., Carlson, C. A., and Knap, A. H.: Carbon-cycle imbalances in the Sargasso Sea, Nature, 372(6506), 537, 1994.

Mikkelsen, N.: On the origin of *Ethmodiscus* ooze, Marine Micropaleontology, 2, 35-46, 10.1016/0377-8398(77)90004-4, 1977.

Moore, J. K., Doney, S. C., and Lindsay, K.: Upper ocean ecosystem dynamics and iron cycling in a global three-dimensional model, Global Biogeochemical Cycles, 18(4), 2004.

Moore, J. K., and Villareal, T. A.: Size-ascent rate relationships in positively buoyant marine diatoms, Limnology and Oceanography, 41(7), 1514-1520, 1996.

Navarro, G., and Ruiz, J.: Hysteresis conditions the vertical position of deep chlorophyll maximum in the temperate ocean, Global Biogeochemical Cycles, 27(4), 1013-1022, 2013.

Olsen, A., Key, R. M., van Heuven, S., Lauvset, S.K., Velo, A., Lin, X., Schirnick, C., Kozyr, A., Tanhua, T., Hoppema, M., Jutterström, S., Steinfeldt, R., Jeansson, E., Ishii, M., Pérez, F.F., and Suzuki, T.: The Global Ocean Data Analysis Project version 2 (GLODAPv2) - an internally consistent data product for the world ocean, Earth System Science Data, 8, 297-323, 2016.

Paulmier, A., Kriest, I., and Oschlies, A.: Stoichiometries of remineralisation and denitrification in global biogeochemical ocean models, Biogeosciences, 6(5), 923-935, 2009.

Pilskaln, C. H., Villareal, T. A., Dennett, M., Darkangelo-Wood, C., and Meadows, G.: High concentrations of marine snow and diatom algal mats in the North Pacific Subtropical Gyre: Implications for carbon and nitrogen cycles in the oligotrophic ocean, Deep Sea Research Part I: Oceanographic Research Papers, 52(12), 2315-2332, 2005.

Platt, T., Harrison, W. G., Lewis, M. R., Li, W. K., Sathyendranath, S., Smith, R. E., and Vezina, A. F.: Biological production of the oceans: the case for a consensus, Marine Ecology Progress Series, 77-88, 1989.

Ricard, M.: Observations sur les diatomées marines du genre *Ethmodiscus* Castr., Rev. Algol. N.S.O, 10, 56-73, 1970.

Richardson, T. L., Ciotti, A. M., Cullen, J. J., and Villareal, T. A.: Physiological and optical properties of *Rhizosolenia formosa* (Bacillariophyceae) in the context of open-ocean vertical migration, Journal of Phycology, 32(5), 741-757, 1996.

Richardson, T. L., Cullen, J. J., Kelley, D. E., and Lewis, M. R.: Potential contributions of vertically migrating Rhizosolenia to nutrient cycling and new production in the open ocean, Journal of Plankton Research, 20(2), 219-241, 1998.

Ricker, W. E.: Linear regressions in fishery research, Journal of the fisheries board of Canada, 30(3), 409-434, 1973.

Rivkin, R. B., and Anderson, M. R.: Inorganic nutrient limitation of oceanic bacterioplankton, Limnology and Oceanography, 42(4), 730-740, 1997.

Rivkin, R. B., Swift, E., Biggley, W. H., and Voytek, M. A.: Growth and carbon uptake by natural populations of oceanic dinoflagellates *Pyrocystis noctiluca* and *Pyrocystis fusiformis*, Deep Sea Research Part A. Oceanographic Research Papers, 31(4), 353-367, 1984.

Semina, H. J., and Levashova, S. S.: The biogeography of tropical phytoplankton species in the Pacific Ocean, Int. Rev. Gesamten Hydrobiol., 78, 243-262, 1993.

Semina, H. J., Belyayeva, T. V., Zernova, V. V., MovChan, O. A., Sanina, L. V., Sukhanova, I. N., and Tarkhova, I. A.: Distribution of indicator species of planktonic algae in the World Ocean, Oceanology, 17, 573-579, 1977.

Shipe, R. F., Brzezinski, M. A., Pilskaln, C., and Villareal, T. A.: *Rhizosolenia* mats: An overlooked source of silica production in the open sea., Limnology and Oceanography, 44, 1282-1292, 1999.

Shulenberger, E., and Reid, J. L.: The Pacific shallow oxygen maximum, deep chlorophyll maximum, and primary productivity, reconsidered, Deep Sea Research Part A. Oceanographic Research Papers, 28(9), 901-919, 1981.

Singler, H. R., and Villareal, T. A.: Nitrogen inputs into the euphotic zone by vertically migrating *Rhizosolenia* mats, Journal of Plankton Research, 27(6), 545-556, 2005.

Steemann Nielsen, E.: Über die vertikale Verbreitung der Phytoplanktonten im Meere, Internationale Revue der gesamten Hydrobiologie und Hydrographie, 38, 421-440, 10.1002/iroh.19390380124, 1939.

Sukhanova, I. N., and Rudyakov, Y. A.: Population composition and vertical distribution of *Pyrocystis pseudonoctiluca* (W. Thomson) in the western equatorial Pacific, in: Life activities of pelagic communities in the ocean., edited by: Vinogradov, M. E., Israeli Program Scientific Translation. Jerusalem., 218-228, 1973.

Sukhanova, V. N.: Vertical distribution of some peridinians in the equatorial Pacific Ocean, in: Life activities of pelagic communities in the ocean., edited by: Vinogradov, M. E., Israeli Program Scientific Translation. Jerusalem., 210-217, 1973.

Swift, E.: The marine diatom *Ethmodiscus rex*: its morphology and occurrence in the plankton of the Sargasso Sea, J. Phycol., 2, 456-460, 1973.

Swift, E., Biggley, W. H., and Seliger, H. H.: Species of oceanic dinoflagellates in genera *Dissodinium* and *Pyrocystis*: Interclonal and interspecific comparisons of coloar and photon yield of bioluminscence, Journal of Phycology, 9, 420-426, 10.1111/j.0022-3646.1973.00420.x, 1973.

Swift, E., Meunier, V. A., Biggley, W. H., Hoarau, J., and Barras, H.: Factors affecting bioluminescence capacity in oceanic dinoflagellates, in: Bioluminescence: current perspectives, edited by: Nealson, K. H., Burgess Publishing Co., Minneapolis, 95-106, 1981.

Swift, E., Stuart, M., and Meunier, V.: The *in situ* growth rates of some deep-living oceanic dinoflagellates: *Pyrocystis fusiformis* and *Pyrocystis noctiluca*, Limnology and Oceanography, 21, 418-426, 1976.

Takahashi, T., Broecker, W. S., and Langer, S.: Redfield ratio based on chemical data from isopycnal surfaces, Journal of Geophysical Research: Oceans, 90(C4), 6907-6924, 1985.

Teng, Y. C., Primeau, F. W., Moore, J. K., Lomas, M. W., and Martiny, A. C.: Global-scale variations of the ratios of carbon to phosphorus in exported marine organic matter, Nature Geoscience, 7(12), 895, 2014.

Toggweiler, J. R.: Carbon overconsumption, Nature, 363(6426), 210, 1993.

Toggweiler, J. R.: Vanishing in Bermuda, Nature, 372(6506), 505, 1994.

Trujillo-Ortiz, A. and Hernandez-Walls, R.: gmregress: Geometric Mean Regression (Reduced Major Axis Regression), A MATLAB file, http://www.mathworks.com/matlabcentral/fileexchange/27918-gmregress, 2010.

Venrick, E. L.: The distribution and ecology of oceanic diatoms in the North Pacific, Ph.D., University of California, San Diego. 684 pp., 1969.

Villareal, T. A.: Abundance of the giant diatom *Ethmodiscus* in the southwest Atlantic Ocean and central Pacific gyre, Diatom Research, 8, 171-177, 1993.

Villareal, T. A.: Single-cell pulse amplitude modulation fluorescence measurements of the giant diatom Ethmodiscus (Bacillariophyceae), Journal of Phycology, 40, 1052-1061, 10.1111/j.1529-8817.2004.03208.x, 2004.

Villareal, T. A., Altabet, M. A., and Culver-Rymsza, K.: Nitrogen transport by vertically migrating diatom mats in the North Pacific Ocean, Nature, 363(6431), 709, 1993.

Villareal, T. A., and Carpenter, E. J.: Chemical composition and photosynthetic characteristics of *Ethmodiscus rex* (Bacillariophyceae): Evidence for vertical migration, Journal of Phycology, 30, 1-8, 1994.

Villareal, T. A., and Carpenter, E. J.: Nitrogen-fixation, suspension characteristics and chemical composition of *Rhizosolenia* mats in the central North Pacific Gyre, Biological Oceanography, 6, 327-345, 1989.

Villareal, T. A., Joseph, L., Brzezinski, M. A., Shipe, R. F., Lipschultz, F., and Altabet, M. A.: Biological and chemical characteristics of the giant diatom *Ethmodiscus* (Bacillariophyceae) in the central North Pacific gyre, Journal of Phycology, 35, 896-902, 1999a.

Villareal, T. A., and Lipschultz, F.: Internal nitrate concentrations in single cells of large phytoplankton from the Sargasso Sea, Journal of Phycology, 31(5), 689-696, 1995.

Villareal, T. A., McKay, R. M. L., Al-Rshaidat, M. M. D., Boyanapalli, R., and Sherrell, R. M.: Compositional and fluorescence characteristics of the giant diatom *Ethmodiscus* along a 3000 km

transect (28 N) in the central North Pacific gyre, Deep Sea Research Part I: Oceanographic Research Papers, 54(8), 1273-1288, 2007.

Villareal, T. A., Pilskaln, C., Brzezinski, M., Lipschultz, F., Dennett, M., and Gardner, G. B.: Upward transport of oceanic nitrate by migrating diatom mats, Nature, 397, 423-425, 1999b.

Villareal, T. A., Pilskaln, C. H., Montoya, J. P., and Dennett, M.: Upward nitrate transport by phytoplankton in oceanic waters: balancing nutrient budgets in oligotrophic seas, PeerJ, 2, e302, 2014.

Villareal, T. A., Woods, S., Moore, J. K., and Culver-Rymsza, K.: Vertical migration of Rhizosolenia mats and their significance to NO3− fluxes in the central North Pacific gyre, Journal of Plankton Research, 18(7), 1103-1121, 1996.

Walker, S. J., Weiss, R. F., and Salameh, P. K.: Reconstructed histories of the annual mean atmospheric mole fractions for the halocarbons CFC-11, CFC-12, CFC-113, and carbon tetrachloride, Journal of Geophysical Research-Oceans, 105(C6), 14285-14296, 2000.

Wallich, G. C.: On microscopic objects collected in India, & c., Transactions of the Microscopical Society of London, 6, 81-87, 1858.

Warner, M. J., and Weiss, R. F.: Solubilities of chlorofluorocarbons 11 and 12 in water and seawater, Deep Sea Research Part A, 32(12), 1485-1497, 1985.

Wiebe, P. H., Remsen, C. C., and Vaccaro, R. F.: *Halosphaera viridis* in the Mediterranean Sea: size range, vertical distribution, and potential energy source for deep-sea benthos, in Deep Sea Research and Oceanographic Abstracts (Vol. 21, No. 8, pp. 657-667), Elsevier, 1974.

Williams, P. J. L. B., Quay, P. D., Westberry, T. K., and Behrenfeld, M. J.: The oligotrophic ocean is autotrophic, Annual review of Marine Science, 5, 535-549, 2013.

Woods, S., and Villareal, T. A.: Intracellular ion concentrations and cell sap density in positively buoyant oceanic phytoplankton, Nova Hedwigia Beihefte, 133, 131, 2008.

Wurl, O., Miller, L., Röttgers, R., and Vagle, S.: The distribution and fate of surface-active substances in the sea-surface microlayer and water column, Marine Chemistry, 115(1-2), 1-9, 2009.

Wurl, O., Miller, L., and Vagle, S.: Production and fate of transparent exopolymer particles in the ocean, Journal of Geophysical Research: Oceans, 116(C7), 2011.

Zweifel, U. L., Norrman, B., and Hagstrom, A.: Consumption of dissolved organic carbon by marine bacteria and demand for inorganic nutrients, Mar. Ecol. Prog. Ser., 101, 23-32, 1993.

Table 1. Residual negative preNO$_3$ (rNPN) and residual positive preNO$_3$ (rPPN) anomaly formation rates at stations ALOHA and BATS.

	Depth (m) or Neutral Density γ^n		f_{DOM}	r_{DOM}	r_{POM}	rNPN		rPPN	
						μmol N m^{-3} d^{-1}	mmol N m^{-2} yr^{-1}	μmol N m^{-3} d^{-1}	mmol N m^{-2} yr^{-1}
ALOHA	0 – 100 m		0.5	18.1	10.6	--	--	2.4 ± 0.8	43.5 ± 10.5
					6.9	--	--	3.3 ± 1.1	61.2 ± 20.2
	24.2 – 24.7		0.5	18.1	10.6	3.0 ± 1.5	17.9 ± 7.4	--	--
					6.9	2.8 ± 1.4	28.3 ± 9.6	--	--
	24.7 – 25.2		0.5	18.9	10.6	2.5 ± 1.4	13.7 ± 7.8	--	--
					6.9	1.6 ± 0.8	18.1 ± 8.8	--	--
Total	r_{POM} = 10.6					--	31.6 ± 10.8	--	--
Total	r_{POM} = 6.9					--	46.4 ± 13.0	--	--
BATS	0 – 80 m		0.4	21.1	10.6	--	--	4.1 ± 0.8	61.8 ± 12.2
					6.9	--	--	5.8 ± 1.2	82.1 ± 13.8
	25.8 – 26.3		0.4	21.1	10.6	3.8 ± 3.1	46.0 ± 39.3	--	--
					6.9	5.5 ± 2.7	87.1 ± 41.0	--	--

Table 2. Contribution of N-poor DOM remineralization to NPN and PPN anomaly formation rates as well as contributions to rNPN and rPPN anomaly formation rates by presumed processes at the time-series sites. NPN/rNPN is for feature on γ^n = 24.2 – 25.2 at station ALOHA and γ^n = 25.8 – 26.3 at the BATS station. Ez PPN/rPPN is for feature at 0 – 100 m depth at station ALOHA and 0 – 80 m depth at the BATS station.

						Proposed attributable process		
Station	$preNO_3$ Feature		N-poor DOM remineralization		Residual $preNO_3$ Feature	TEP production & remineralization	Bacterial nitrate uptake	Phytoplankton vertical migration
ALOHA	NPN		1 – 16 mmol N m^{-2} yr^{-1}		rNPN	16 – 22 mmol N m^{-2} yr^{-1}	0.0 – 3.4 mmol N m^{-2} yr^{-1}	16 – 21 mmol N m^{-2} yr^{-1}
	Ez PPN		2 – 21 mmol N m^{-2} yr^{-1}		Ez rPPN	16 – 22 mmol N m^{-2} yr^{-1}	--	27 – 36 mmol N m^{-2} yr^{-1}
					% rNPN	47 – 50%	0 – 7%	45 – 50%
					% Ez rPPN	37 – 41%	--	59 – 63%
BATS	NPN		1 – 14 mmol N m^{-2} yr^{-1}		rNPN	3.2 – 6.0 mmol N m^{-2} yr^{-1}	0.2 – 3.0 mmol N m^{-2} yr^{-1}	43 – 78 mmol N m^{-2} yr^{-1}
	Ez PPN		2 – 17 mmol N m^{-2} yr^{-1}		Ez rPPN	3.2 – 6.0 mmol N m^{-2} yr^{-1}	--	59 – 76 mmol N m^{-2} yr^{-1}
					% rNPN	6 – 7%	0.5 – 3.5%	90 – 93%
					% Ez rPPN	5 – 7%	--	93 – 95%

Figure 1. (a) Climatology of the residual preNO$_3$ tracer [µM] in the upper 250 m at station ALOHA (22.75 ºN 158 ºW) for a value of r_{POM} = 10.6. Black contour lines show neutral density γ^n = 24.2, 24.7, and 25.2. (b) The monthly averaged residual preNO$_3$ [µM] climatology for all data in years 1989 – 2016.

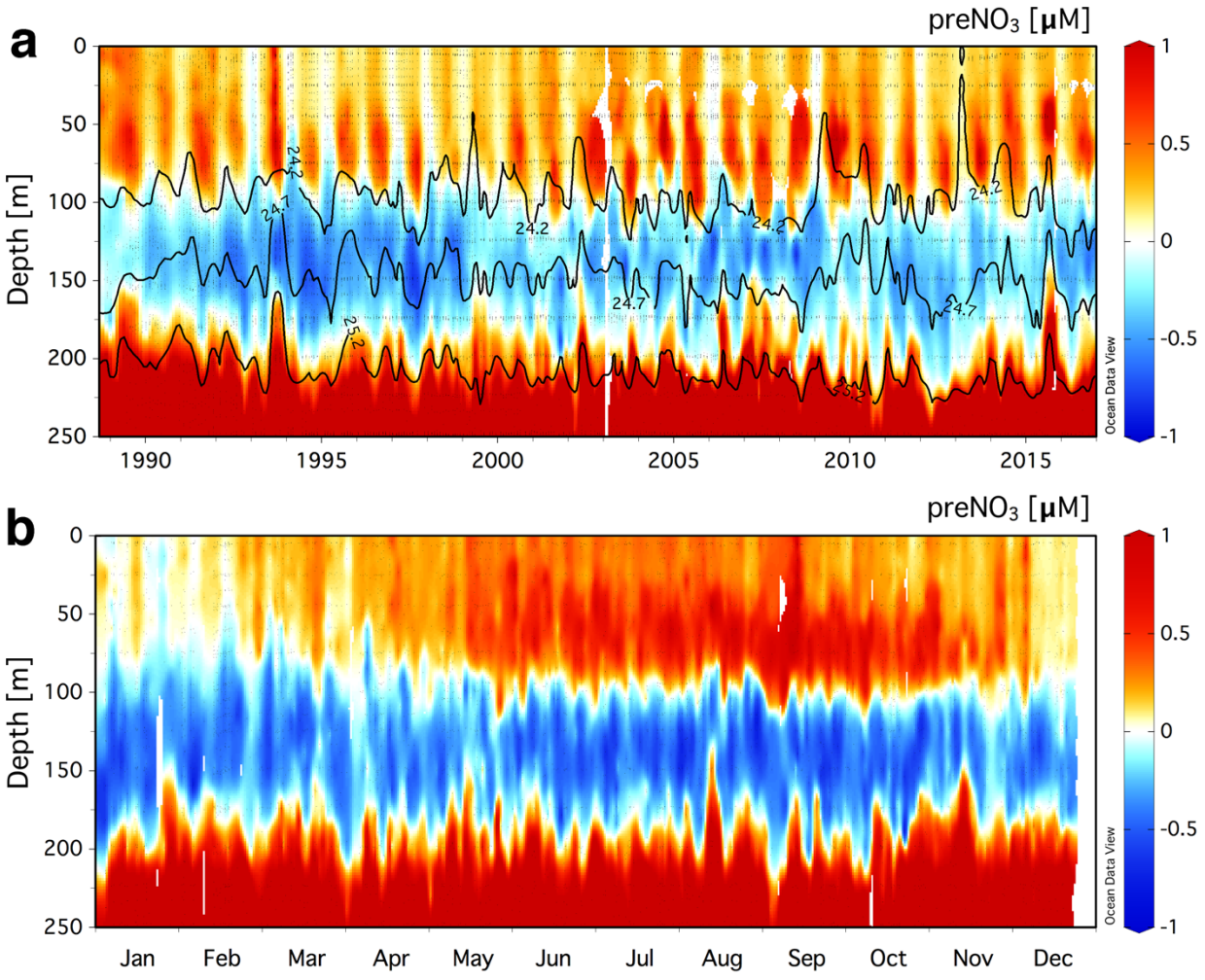

Figure 2. (a) Climatology of the residual preNO$_3$ tracer [µM] in the upper 200 m at the BATS station (31.67 ºN 64.17 ºW) for a value of r_{POM} = 10.6. Black contour lines show neutral density γ^n = 25.8 and 26.3. (b) The monthly averaged residual preNO$_3$ [µM] climatology for all data in years 1993 – 2016.

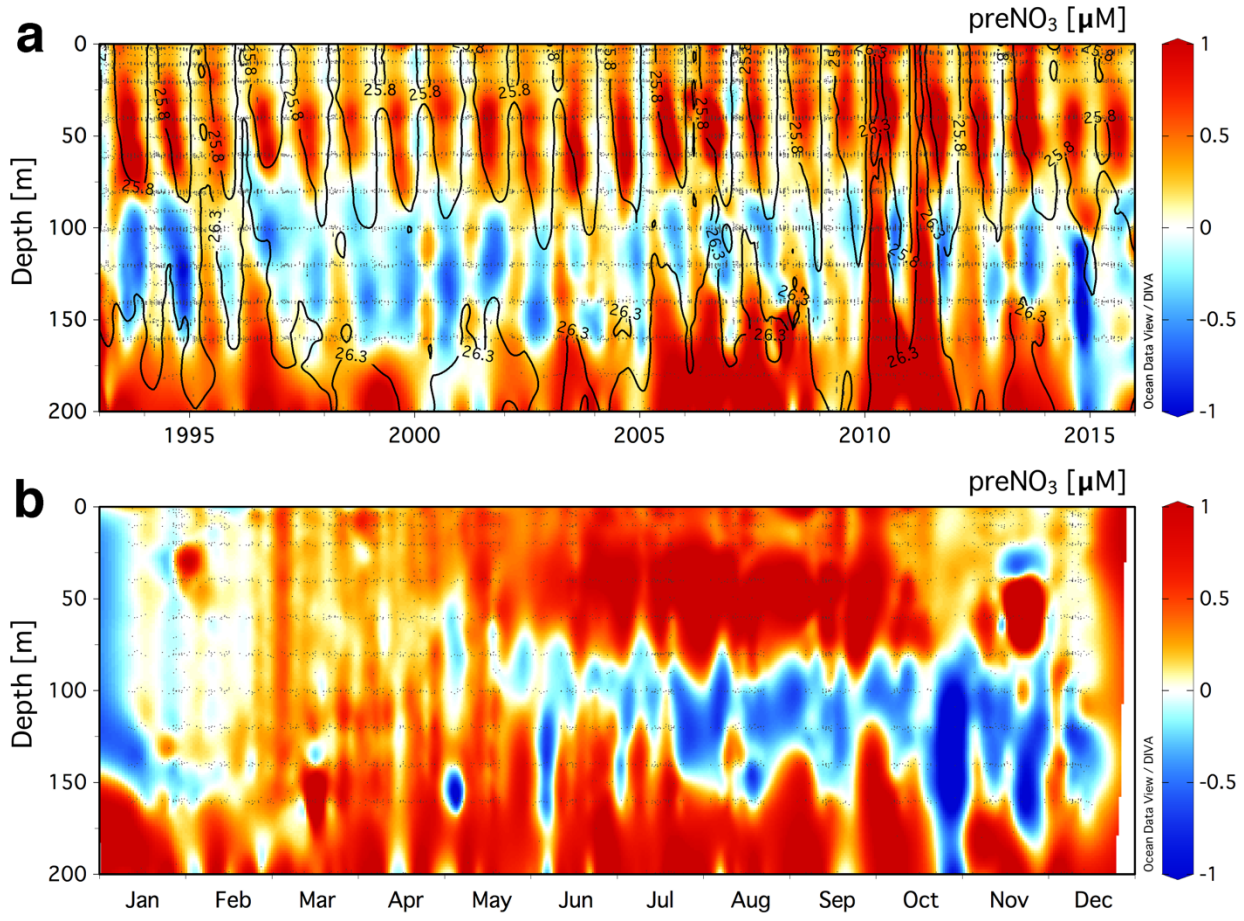

Figure 3. (a) Climatology of the residual $prePO_4$ tracer [µM] in the upper 250 m at station ALOHA (22.75 ºN 158 ºW) for a value of r_{POM} = 10.6. Black contour lines show neutral density γ^n = 24.2, 24.7, and 25.2. (b) The monthly averaged residual $prePO_4$ [µM] climatology for all data in years 1989 – 2016.

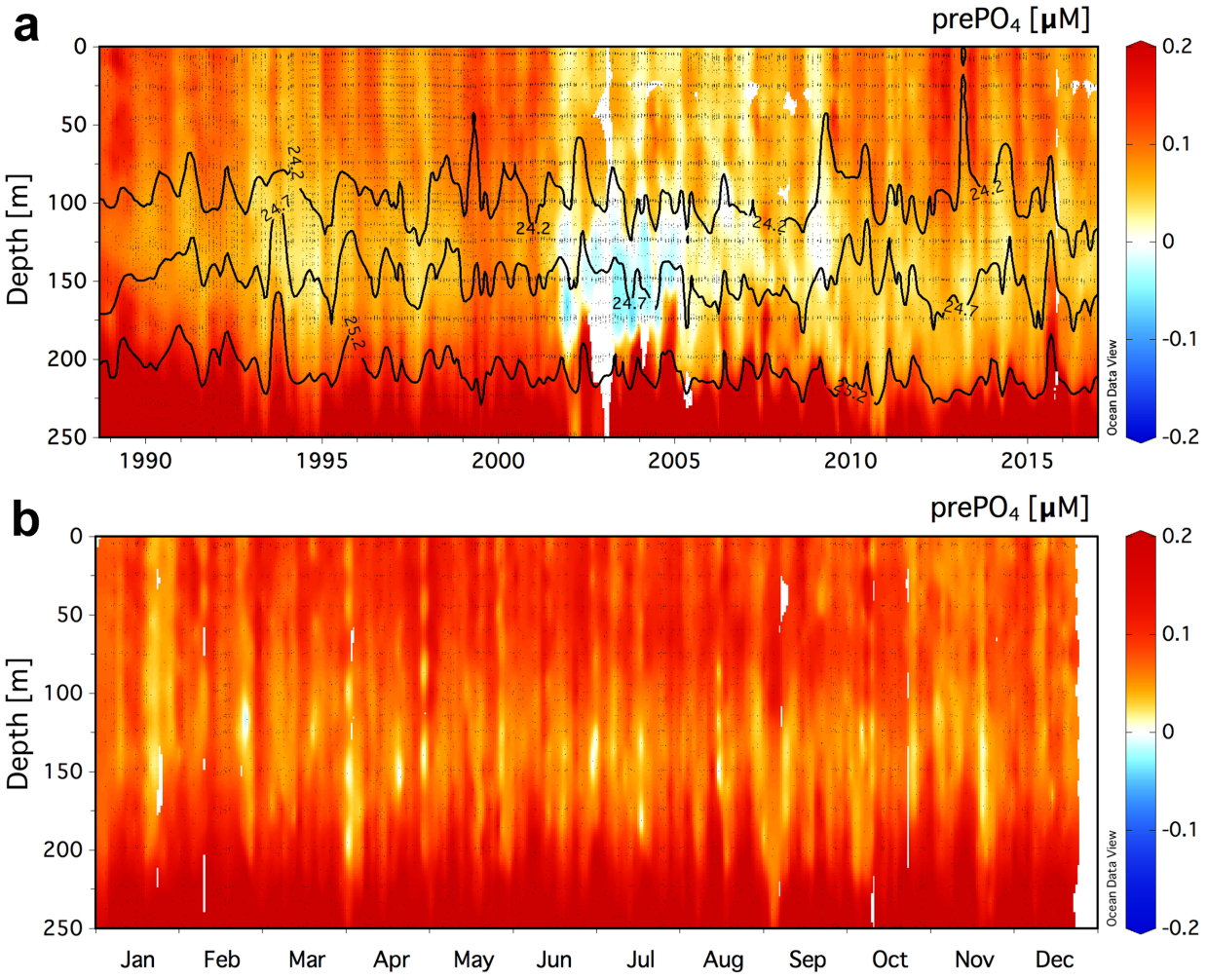

Figure 4. (a) Climatology of the residual $prePO_4$ tracer [µM] in the upper 200 m at the BATS station (31.67 ºN 64.17 ºW) for a value of r_{POM} = 10.6. Black contour lines show neutral density γ^n = 25.8 and 26.3. (b) The monthly averaged residual $prePO_4$ [µM] climatology for all data in years 1993 – 2016.

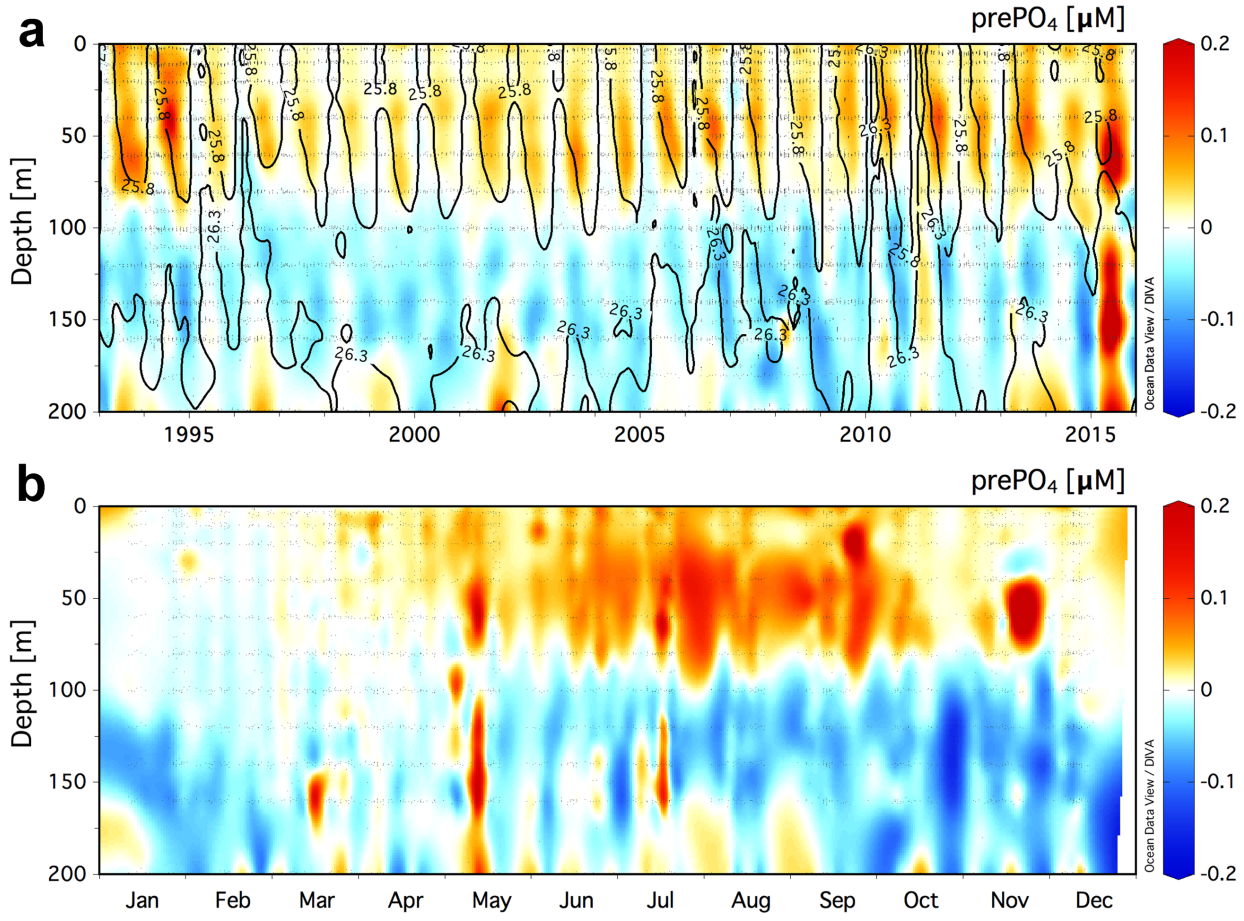

Figure 5. Seasonal climatology of the residual preNO$_3$ tracer [µM] at 150 m depth from the World Ocean Atlas, 2013, 1º climatologies of O_2 anomaly and nitrate. Residual preNO$_3$ is calculated using values of f_{DOM} = 0.5, r_{DOM} = 20.0, and r_{POM} = 8.75.